Journal of Photochemistry & Photobiology, A: Chemistry 461 (2025) 116154

Contents lists available at ScienceDirect

Journal of Photochemistry & Photobiology, A: Chemistry

journal homepage: www.elsevier.com/locate/jphotochem

A copper complex receptor for nanomolar sulfide sensing and applications in DNA/BSA binding

Dipankar Das [a], Aritra Roy [b], Cauê P. Souza [c], Somnath Mondal [a], Sourav Sutradhar [a], Parnashabari Sarkar [a], Felipe Fantuzzi [c,*], Biswa Nath Ghosh [a,*]

[a] Department of Chemistry, National Institute of Technology Silchar, Silchar-788010, Assam, India
[b] Department of Chemical and Energy Engineering, London South Bank University, London SE1 0AA, UK
[c] School of Chemistry and Forensic Science, University of Kent, Park Wood Rd, Canterbury CT2 7NH, UK

ARTICLE INFO

Keywords:
Sulfide sensing
Colorimetric sensors
Real-time detection
DFT calculations
Molecular docking

ABSTRACT

Traditionally toxic sulfide species (S^{2-}, HS^-, and H_2S) play indispensable roles in various biological, environmental, and industrial processes. However, excessive exposure to these species can result in numerous chronic diseases. Considering the importance of sulfide recognition, we have synthesized and characterized a simple 1:1 Cu(II) complex of **L** (**$CuCl_2L$** receptor) based on a substituted 2,6-dipyrazinylpyridine (dppy) moiety (**L** = 4-(2,6-di(pyrazin-2-yl)pyridin-4-yl)-*N*,*N*-dimethylaniline). The complex was analyzed both experimentally and computationally using DFT and TD-DFT calculations. The *in-situ* prepared **$CuCl_2L$** receptor is employed to selectively recognize sulfide species (detection limit: 82.50 nM) in the presence of other anions in higher concentration (ten equivalents of F^-, Cl^-, Br^-, I^-, $CH_3CO_2^-$, HCO_3^-, $H_2PO_4^-$, NO_3^-, SO_3^{2-}, SO_4^{2-}, $S_2O_3^{2-}$, CO_3^{2-}, and HPO_4^{2-} (10 mM)) in aqueous acetonitrile (2:1 v/v, 10 mM HEPES buffer, pH 7.4) through absorption spectral studies. Furthermore, the receptor is successfully utilized for various real-time detection applications and demonstrated significant intercalative binding interaction with Calf–Thymus DNA (CT-DNA) and good binding interactions with bovine serum albumin (BSA), supported by viscometry and molecular docking studies.

1. Introduction

Adequate, effective receptors with optical responses have gathered immense attention for instant anion sensing, as these species play indispensable roles in various environmental, biological, and chemical processes [1–5]. Among them, sulfide species have drawn particular concern due to their widespread dispersion in the environment as a traditional toxic and hazardous pollutant. Sulfide accumulates in water, including domestic wastewater [6,7], from various sources such as crude petroleum, volcanic eruptions, and the reduction of sulfate by anaerobic bacteria [8,9]. It also frequently emerges as a by-product of many industrial processes [10], while offering diverse applications across sectors [11] such as cosmetics [12], dyes [13], sulfuric acid, and wood pulp manufacturing [14].

Once hydrolyzed in water, sulfide is primarily converted into hydrogen sulfide (H_2S) or hydrosulfide (HS^-) [6,7], as aqueous S^{2-} does not exist under typical conditions. This has been confirmed by recent experiments involving Na_2S dissolved in hyper-concentrated NaOH(aq) and CsOH(aq) [15], and further supported by molecular dynamics simulations [16]. The implications of this hydrolysis are profound, as H_2S plays crucial physiological roles [17], including modulation of blood pressure [18], brain neuromodulation [19], regulation of inflammation [20], and suppression of oxidative stress [21]. Furthermore, H_2S has been shown to protect against ischemia/reperfusion injury [22,23], to act as an antioxidant [24], and to scavenge reactive oxygen species [25]. Alterations in cellular H_2S levels have been linked to various diseases, such as Down's syndrome [26], Alzheimer's disease [27], diabetes [22], and liver cirrhosis [28].

Exposure to excessive concentration of sulfide can cause several metabolic and physiological issues, ranging from irritation in mucous membranes [29] and unconsciousness [30] to respiratory paralysis [31]. While H_2S is essential in low concentrations, its toxicity increases at higher levels, leading to permanent brain damage [32–34] and even death through asphyxiation [35]. Given its dual role as both a necessary biological molecule and a toxic hazard, the detection of sulfide species is of critical importance across biological, environmental, and industrial

* Corresponding authors.
E-mail addresses: f.fantuzzi@kent.ac.uk (F. Fantuzzi), bnghosh@che.nits.ac.in (B.N. Ghosh).

https://doi.org/10.1016/j.jphotochem.2024.116154
Received 11 September 2024; Received in revised form 12 October 2024; Accepted 9 November 2024
Available online 13 November 2024

fields.

In recent years, the metal displacement approach utilizing copper receptors for sulfide detection has attracted extraordinary attention [36]. This method is based on the principle that sulfide can displace Cu (II) ions from a copper receptor. This displacement results in the formation of a highly stable CuS compound, characterized by its remarkably low solubility product constant ($K_{sp} = 6.3 \times 10^{-36}$) [37]. The formation of this stable moiety is a key indicator in the successful detection of sulfide [8,12,38]. Furthermore, copper complexes possess less toxic side effects than those based on exogenous metals [39]. In addition to their role in sulfide detection, they also exhibit potential antioxidant, antibacterial, and antitumor/anti-cancer activities [40–42]. Among the various receptor systems currently available for sulfide recognition, several encounter specific limitations, such as multi-step synthetic procedure requiring stringent synthetic conditions [43–46], notably low solubility in aqueous media [12,47,48], potential interference from other S-containing moieties [49], among others. These challenges underscore the need for more streamlined and selective approaches in the development of sulfide detection methodologies.

Nitrogen-based heterocyclic ligands such as 2,2′:6′,2″-terpyridine, 2,6-dipyrazinylpyridine (dppy), and their transition metal complexes have received considerable interest for their integration into a diverse array of applications. These range from halogen bonding [50,51] and protein interaction to drug-displacement studies [52], hydrogelation [53,54], self-assembly [55], anions sensing [56,57], and amino acids sensing [58], to name a few. The growing popularity of these compounds can be attributed to their straightforward synthesis, high stability, and their exceptional electrochemical and photophysical properties [59–61]. Considering practicality and convenience, various detection techniques have been utilized to recognize sulfide species [33,62–65]. Among these, colorimetric and spectroscopic methods, particularly UV–Visible (UV–Vis) spectroscopy, have attracted the most attention. Their popularity stems from several key advantages: high accuracy, cost-effectiveness, rapid response, swift processing, operational simplicity, and the ability for on-site detection [66–68].

Herein, we have prepared a simple Cu-dppy receptor (dppy: 2,6-dipyrazinylpyridine), specifically a Cu(II) complex (**$CuCl_2$L**) of the 4-(2,6-di(pyrazin-2-yl)pyridin-4-yl)-*N*,*N*-dimethylaniline ligand (**L**). Similar to other dppy-based ligands, **L** demonstrates strong binding interactions with various 3d transition metal ions, including Cu(II) and Zn (II). We selected **$CuCl_2$L** for sulfide ion detection due to the pronounced interactions between Cu(II) and sulfide ions (*vide supra*). The **$CuCl_2$L** receptor was characterized using UV–Vis, Fourier-transform infrared (FT-IR), and electron spin resonance (ESR) spectroscopies, along with high-resolution mass spectrometry (HRMS). The *in-situ* synthesized **$CuCl_2$L** receptor demonstrates exceptional selectivity in detecting sulfide species at nanomolar concentrations, with a detection limit of 82.50 nM. This was achieved even in the presence of various other anions at higher concentrations (ten equivalents) such as F^-, Cl^-, Br^-, I^-, $CH_3CO_2^-$, HCO_3^-, $H_2PO_4^-$, NO_3^-, SO_3^{2-}, SO_4^{2-}, $S_2O_3^{2-}$, CO_3^{2-}, and HPO_4^{2-}, in an aqueous acetonitrile environment (2:1 v/v, 10 mM HEPES) maintained at a physiological pH of 7.4. Additionally, this *in-situ* prepared **$CuCl_2$L** receptor is effectively utilized in various real-time sulfide detection applications. Particularly, it is employed to study Calf–Thymus DNA (CT-DNA) and bovine serum albumin (BSA) interactions with the help of absorption, emission, and molecular docking study.

2. Experimental section

2.1. Materials and methods

Spectroscopic and analytical grade chemicals used in the synthesis and spectral analyses were obtained commercially. ^{1}H NMR, ESI-HRMS, ESR, and FT-IR spectra were acquired using the JEOL ECZ500R/S1 NMR spectrometer, the Impact HD UHR-TOF mass spectrometer, the JES-FA200 (JEOL) ESR spectrometer, and the 3000 Hyperion FT-IR spectrometer (Bruker, Germany), respectively. Absorption and emission spectra were recorded using the Mortas Scientific UV plus MSGUI3.1.0 absorption spectrophotometer and the HITACHI-F4600 Fluorescence spectrophotometer, respectively.

2.2. Synthesis of the Cu(II) complex of L ($CuCl_2$L)

The 4-(2,6-di(pyrazin-2-yl)pyridin-4-yl)-*N*,*N*-dimethylaniline ligand **L** was synthesized following an available synthetic procedure [69] (see the Supplementary Information, SI, for the synthetic procedure and synthetic scheme of **L**). An ethanolic solution of $CuCl_2$ (26.8 g, 0.2 mmol, 10 mL) was added to a dichloromethane solution of the synthesized **L** (0.148 g, 0.4 mmol, 10 mL), and stirring the reaction mixture at room temperature for 2 h yielded a dark red-colored precipitate. The precipitate was collected and washed with ethanol (30 mL) several times, resulting in 1:1 Cu(II) complex of L (**$CuCl_2$L**). Yield: 85%. ESI-MS: [**CuClL**]$^+$ *m/z* 452.0571 (found); 452.0577 (calculated). Elemental analysis ($C_{21}H_{18}Cl_2CuN_6$ g mol^{-1}): C 51.60; H 3.71; N 17.19 (calculated); C 51.41; H 3.55; N 17.02 (found). FT-IR (υ_{max}/cm^{-1}): 3047, 3002, 2820, 1580, 1462, 1399, 1357, 1232, 1170, 1075, 834 (see Figs. S1–S6 in the SI for ^{1}H NMR, HRMS, FT-IR, and EPR spectral plots of the ligand **L** and **$CuCl_2$L**).

2.3. Preparation of experimental solutions

2.3.1. Uv–vis absorption spectral studies

An acetonitrile solution of **L** (115 μM, 25 mL) was prepared, along with aqueous solutions of various anions. These included sodium salts of S^{2-} (1 mM Na_2S, 50 mL), F^-, Cl^-, Br^-, I^-, $CH_3CO_2^-$, HCO_3^-, $H_2PO_4^-$, NO_3^-, SO_3^{2-}, SO_4^{2-}, $S_2O_3^{2-}$, CO_3^{2-}, and HPO_4^{2-} (10 mM, 50 mL). The **$CuCl_2$L** receptor (38 μM, 10 mL) solution was prepared *in-situ* by mixing an aqueous $CuCl_2$ solution (1 mM, 1.15 mL) and an acetonitrile solution of **L** (115 μM, 10 mL), followed by dilution with an aqueous HEPES buffer (10 mM, 20 mL, pH 7.4).

2.3.2. DNA binding studies

A stock solution of CT-DNA was prepared by dissolving it in aqueous HEPES buffer (10 mM, pH 7.4) and allowing it to stand overnight at 4 °C. This stock solution exhibited an absorption band intensity ratio of 1.90:1 (for absorption bands 260 nm and 280 nm), indicating it was sufficiently free from protein. The concentration of CT-DNA was determined from the intensity of the 260 nm absorbance band and extinction coefficient $\varepsilon_{260} = 6600$ M^{-1} cm^{-1} [70]. Absorption spectral titration was carried out by gradually adding a CT-DNA (0–260 μM) solution to an *in-situ* prepared **$CuCl_2$L** receptor (38 μM, 1.5 mL) in aqueous HEPES buffer (10 mM, pH 7.4). The **$CuCl_2$L** (38 μM, 1.5 mL) receptor was prepared as in section 2.3.1. The binding constant (K_b) [71] was determined from the absorption spectral titration using the Wolfe-Shimmer Equation (1) [72]:

$$[\text{CT-DNA}]/(\varepsilon_a - \varepsilon_f) = [\text{CT-DNA}]/(\varepsilon_b - \varepsilon_f) + 1/K_b(\varepsilon_b - \varepsilon_f) \quad (1)$$

where [CT-DNA] is the CT-DNA concentration, ε_a is the absorption intensity/[**$CuCl_2$L**] (with [**$CuCl_2$L**] being the **$CuCl_2$L** receptor concentration), ε_f is the extinction coefficient of free **$CuCl_2$L**, and ε_b is the extinction coefficient of the fully bound **$CuCl_2$L** to DNA.

Ethidium bromide (EB), a standard DNA intercalating reagent, was used for the CT-DNA emission spectral titration study. In this experiment, an *in-situ* prepared **$CuCl_2$L** (100 μM, 50 μL) receptor was gradually added to an equimolar mixture of CT-DNA and EB (45 μM, 2 mL). The fluorescence quenching constant (K_{SV}) [73] and the binding constant (K_{app}) [74] were determined from the emission spectral titration using the Stern–Volmer equation (2) and equation (3), respectively:

$$\frac{F_0}{F} = 1 + K_{SV}[\mathbf{CuCl_2L}] \quad (2)$$

$$K_{app} \times [\mathbf{CuCl_2L}]_{1/2} = K_{EB} \times [\mathrm{EB}] \quad (3)$$

where F_0 is the fluorescence intensity in the absence of **$CuCl_2L$** receptor, F is the fluorescence intensity in the presence of **$CuCl_2L$** receptor, K_{SV} is the linear Stern–Volmer constant, $[\mathbf{CuCl_2L}]_{1/2}$ is the **$CuCl_2L$** receptor concentration at 50 % reduction of fluorescence intensity, K_{EB} is 10×10^6 M^{-1}, and [EB] is 40 μM.

2.3.3. BSA binding study

A BSA stock solution was prepared for a binding interaction study with the **$CuCl_2L$** receptor. For absorption and emission spectral studies, the **$CuCl_2L$** receptor (90 μM, 20 μL) was gradually added to BSA (2.5 μM, 2 mL) in phosphate buffer (100 mM, pH 7.4). The quenching constant (K_{SV}) [75] and affinity constant (K) [76] were calculated by using equation (2) and the Scatchard equation (4), respectively:

$$\log(F_0 - F)/F = \log K + n\log[\mathbf{CuCl_2L}] \quad (4)$$

where K is the affinity constant of the **$CuCl_2L$** receptor with BSA, and n is the number of binding sites per albumin or binding stoichiometry.

2.3.4. Viscometry titration study

A stock solution of **$CuCl_2L$** receptor (100 μM, 0.7 mL) was gradually added to a CT-DNA solution (25 μM, 28 mL), and a viscometry titration study was carried out using an Ostwald viscometer. The average flow time of the solutions was measured using a digital stopwatch. The relative viscosity values were determined using the expression $\eta = (t - t_0)/t_0$, where t and t_0 represent the observed flow time of the CT-DNA and buffer solution, respectively. These values were presented as $(\eta/\eta_0)^{1/3}$ vs. [**$CuCl_2L$**]/[CT-DNA] binding ratio, where η denotes the viscosity of CT-DNA in the presence of **$CuCl_2L$**, and η_0 represents the viscosity of CT-DNA alone [71,77].

2.4. Molecular docking study

The Autodock 4.2 software [78] was employed for docking studies, wherein the ground state energy-optimized structure of the **$CuCl_2L$** receptor was docked with the crystal structures of CT-DNA (PDB ID: 1BNA) and BSA (PDB ID: 4F5S). The following line was added to the parameters files to include the copper atom parameters in AutoDock 4.2: "atom_par Cu 3.50 0.005 12.000—0.00110 0.0 0.0 0—1 −1 4 # Non H-bonding". The docking results were then visualized and analyzed using the Discovery Studio 3.5 software [79].

2.5. DFT calculations

Quantum chemical analyses for our study were performed using the Gaussian 16 software, Revision C.01 [80]. Building on insights from our previous work [81] with another dppy-based Cu(II) complex, we optimized geometries using the PBE0 [82,83] functional, integrating the D3 (BJ) [84,85] approach for dispersion corrections. The def2-TZVP basis set was employed on the Cu atom, while the def2-SVP basis set was applied to all the others [86]. This selection is labelled as bs1, making the theory level PBE0-D3(BJ)/bs1. The unrestricted Kohn–Sham method was used for open-shell systems. Gibbs free energy corrections, obtained in calculations at the PBE0-D3(BJ)/bs1 level, were applied to single-point energy computations using the PBE0-D3(BJ) functional but with an expanded basis set. Here, def2-TZVP was used for all elements except Cu, which was treated using the def2-QZVP basis set, a combination referred to as bs2. Solvation effects were incorporated via the solvent model based on density (SMD) [87], considering a 2:1 water/acetonitrile solvent mixture. Consequently, free energy calculations were conducted at the SMD/PBE0-D3(BJ)/bs2 level of theory. To ensure accuracy in associative and dissociative steps, a concentration correction of $\Delta G^{0\rightarrow *} = 1.89$ kcal/mol was applied to the free energy values of all computed species, compensating for standard state variations from gas phase (1 atm) to condensed phase (1 M) [88–90]. All optimized geometries were verified as minima on their respective potential energy surfaces, confirmed by vibrational frequency calculations that showed only positive eigenvalues in the Hessian matrices. Finally, time-dependent DFT (TD-DFT) calculations were performed using the SMD/PBE0-D3(BJ)/bs1 level of theory. A total of 50 excited electronic states were considered in the calculations. The nature of key electronic transitions was examined through the charge density difference (CDD) analysis and the interfragment charge transfer (IFCT) method, as implemented in Multiwfn 3.8 [91]. Further insights into the excited state properties were obtained using the TheoDORE program [92]. A Gaussian envelope was used to shape the vertical excitations in all TD-DFT spectra, as described by the following equation:

$$\epsilon(\lambda) = \sum\nolimits_i \epsilon_i^{max} \exp\left[\left(\frac{1/\lambda - 1/\lambda_i}{1/\sigma}\right)^2\right] \quad (5)$$

where

$$\epsilon_i^{max} = \frac{\sqrt{\pi} \times e \times N}{1000 \times \ln 10 \times c \times m_e} \times \frac{f_i}{10^7/\sigma} \quad (6)$$

In Equation (5), $\epsilon(\lambda)$ is the molar absorptivity, which depends on the wavelength, and is expressed in units of $L\,mol^{-1}cm^{-1}$. The variables λ and λ_i refer to the wavelength (independent variable) and wavelength of the i-th transition (the center of the Gaussian), respectively, with both measured in nm. The Gaussian standard deviation, σ, is also expressed in nm, ensuring that the exponent remains dimensionless. Equation (6) rescales the oscillator strength f_i (dimensionless) for each i-th electronic transition into molar absorptivity. The factor of 10^7 is included to convert $1/\sigma$ to cm^{-1}, while the factor of 1000 converts cm^3 to L. In this formula, e represents the elementary charge (in esu), N is Avogadro's constant (in mol^{-1}), c is the speed of light (in cm s^{-1}), and m_e is the electron mass (in g). The value of $\sigma = 6200$ nm, which corresponds to 0.2 eV, was used in the calculations.

3. Results and discussion

3.1. Synthesis and sulfide sensing analysis of $CuCl_2L$

The ligand **L**, upon reaction with $CuCl_2$ in a dichloromethane-ethanol solvent mixture, successfully yielded the **$CuCl_2L$** complex at room temperature, as outlined in Scheme 1. The complex was characterized using a range of techniques including ^{1}H NMR, HRMS, elemental analysis, ESR, and FT-IR (see Figs. S1–S7 in the SI). This **$CuCl_2L$** complex is expected to have a distorted square-pyramidal geometry. In this structure, the Cu(II) ion is penta-coordinated, involving three nitrogen atoms from the substituted dppy moiety and two chloride anions. Our DFT calculations confirm this geometric configuration (see Scheme 1), revealing that the optimized structure of **$CuCl_2L$** exhibits a structural parameter τ value [93] of 0.098. A τ value of 0 indicates a perfect square-pyramidal geometry, while a value of 1 corresponds to a perfect trigonal bipyramid. Additionally, the ESR spectrum of the complex, displaying a $g\| > g_\perp > 2.002$ value [34], further corroborates this geometry (see Fig. S7 in the SI). Similar distorted square-pyramidal geometrical arrangements have been observed in other Cu(II)-dppy complexes [94–96].

The UV–Vis spectra of **L** (38 μM, 1.5 mL) in aqueous acetonitrile (2:1 v/v, 10 mM HEPES buffer, pH 7.4) before and after the addition of $CuCl_2$ is depicted in Fig. 1a. **L** exhibits two prominent absorption bands at 233 nm and 295 nm, accompanied by a shoulder at 364 nm. The computed UV–Vis spectrum of **L** obtained from TD-DFT calculations (see Fig. 1b and additional Figs. S9–S10 and Tables S1 and S2 in the SI) shows excellent agreement with the experimental spectrum, with the three main electronic excitations occurring at 235 nm, 282 nm, and 378 nm. The first excitation is attributed to a mixed π → π* and n → π* transition

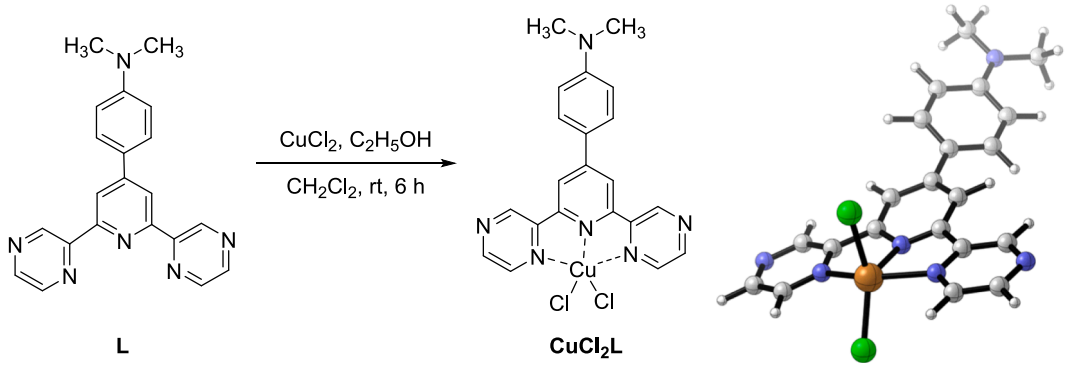

Scheme 1. Preparation of **$CuCl_2L$**, the Cu(II) complex of **L**, and its optimized structure.

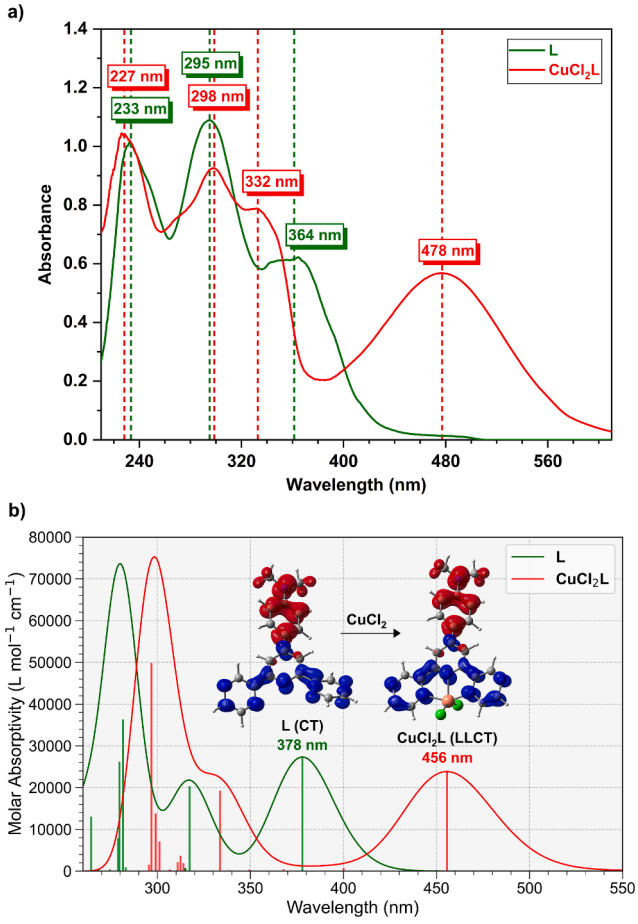

Fig. 1. (a) Absorption spectra of **L** (38 μM, 1.5 mL) and the *in-situ* prepared **$CuCl_2L$** receptor (38 μM, 1.5 mL) in aqueous acetonitrile (2:1 v/v, 10 mM HEPES, pH 7.4). (b) Computed TD-DFT absorption spectra of **L** and **$CuCl_2L$** at the SMD/PBE0-D3(BJ)/bs1 level. The insets show the charge density difference (CDD) plots of the charge transfer (CT) excitation of **L** at 378 nm and the corresponding ligand-to-ligand charge transfer (LLCT) excitation of **$CuCl_2L$** at 456 nm. In the CDD plots, charge flows from red to blue. Isovalues: 0.002 a.u.

with local excitation (LE) character, primarily involving the pyrazole and pyridine rings. The latter two excitations are associated with charge transfer (CT) transitions from the aniline ring to the nitrogen-bearing rings.

Upon the addition of aqueous $CuCl_2$ to **L**, the *in-situ* prepared **$CuCl_2L$** complex exhibited two prominent absorption bands at 227 nm and 298 nm, with a shoulder at 332 nm and a new absorption band emerging at 478 nm. TD-DFT calculations reveal that the band at 478 nm (computed at 456 nm) shares the same characteristics as the 364 nm band of the free ligand **L** but is redshifted due to metal coordination. The IFCT analysis indicates that this transition possesses an 86% CT character, with 89% of the hole density localized on the aniline group and 10% on the pyrazole/pyridine rings. The electron density is predominantly localized on the nitrogen-bearing rings (91%), with only 3.5% at the $CuCl_2$ center. A similar distribution is observed in the electron-hole correlation plots (see Figs. S9–S10 in the SI). Thus, the transition observed at 478 nm is identified as a ligand-to-ligand charge transfer (LLCT), rather than metal-to-ligand charge transfer (MLCT). The presence of this transition in the experimental spectrum confirms the successful formation of the *in-situ* **$CuCl_2L$** complex in aqueous acetonitrile. Moreover, DFT calculations further corroborate the favorable formation of the **$CuCl_2L$** complex from **L** and $CuCl_2$ in aqueous acetonitrile, with a computed free energy change (ΔG) of –32.5 kcal mol^{-1}.

To evaluate the selectivity of the **$CuCl_2L$** receptor for anion sensing, separate aqueous solutions of various anions were tested. These included S^{2-} (Na_2S 1 mM, 40 μL) and a range of other anions such as F^-, Cl^-, Br^-, I^-, $CH_3CO_2^-$, HCO_3^-, $H_2PO_4^-$, NO_3^-, SO_3^{2-}, SO_4^{2-}, $S_2O_3^{2-}$, CO_3^{2-}, and HPO_4^{2-} (each at 10 mM, 57 μL concentration). Each anion solution was individually added to a solution of the **$CuCl_2L$** receptor (38 μM, 1.5 mL) prepared in aqueous acetonitrile (2:1 v/v, 10 mM HEPES, pH 7.4). Following the addition of these anions, the absorption spectra were recorded to assess the receptor's response and its ability to selectively detect each anion under these conditions.

Upon adding the anions (ten equivalents) specified earlier (excluding Na_2S), there was no significant alteration observed in the absorption spectrum of the **$CuCl_2L$** receptor, as depicted in Fig. 2. Contrarily, the introduction of just one equivalent of Na_2S to the *in-situ* prepared **$CuCl_2L$** receptor led to a notable change: the near disappearance of the LMCT absorption band at 478 nm. Subsequently, the absorption spectrum of the **$CuCl_2L$** receptor shifted to closely resemble that of the free ligand **L**, also shown in Fig. 2.

The observed absorption spectral behavior indicates that the addition of Na_2S effectively facilitates the decomplexation of the Cu(II) moiety from the **$CuCl_2L$** receptor. This decomplexation occurs due to the strong binding interaction between the sulfide ions and the Cu(II) ion, leading to the displacement of Cu(II) from the complex. Consequently, **L** is released in the solution, while the sulfide precipitates as CuS given its very low solubility product constant. This mechanism highlights the selective sensing of sulfide by the *in-situ* prepared **$CuCl_2L$** receptor in an aqueous acetonitrile medium, demonstrating its potential as a practical sensor for this specific species.

In order to investigate the **$CuCl_2L$** receptor's interaction dynamics and sensitivity to sulfide species, an absorption spectral titration study was performed. This involved the incremental addition of S^{2-} (Na_2S 0.1 mM, 4 μL) to the *in-situ* prepared **$CuCl_2L$** receptor solution (38 μM, 1.7 mL) in aqueous acetonitrile (2:1 v/v, 10 mM HEPES, pH 7.4), as illustrated in Fig. 3. Each addition of the anion induced noticeable hypochromic shifts in the 298 nm absorption band, including its shoulder at

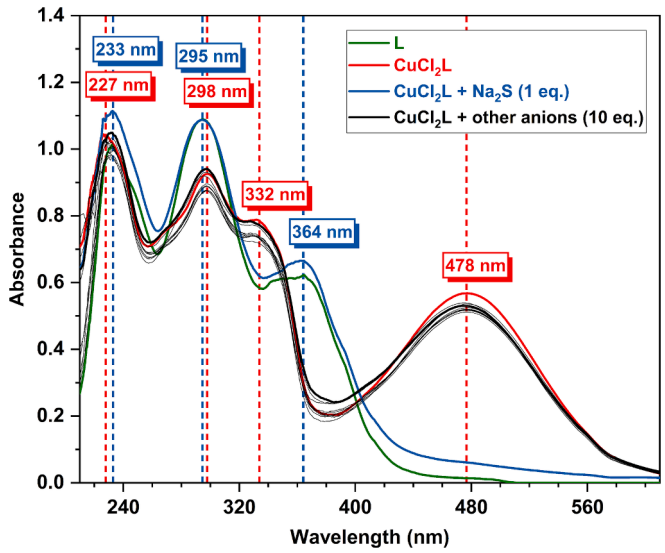

Fig. 2. Absorption spectra of the *in-situ* prepared **$CuCl_2L$** receptor (38 μM, 1.5 mL) upon addition of one equivalent S^{2-} (Na_2S 1 mM, 57 μL) and ten equivalent different anions (F^-, Cl^-, Br^-, I^-, $CH_3CO_2^-$, HCO_3^-, $H_2PO_4^-$, NO_3^-, SO_3^{2-}, SO_4^{2-}, $S_2O_3^{2-}$, CO_3^{2-}, and HPO_4^{2-}) (10 mM, 57 μL) in aqueous acetonitrile (2:1 v/v, 10 mM HEPES, pH 7.4).

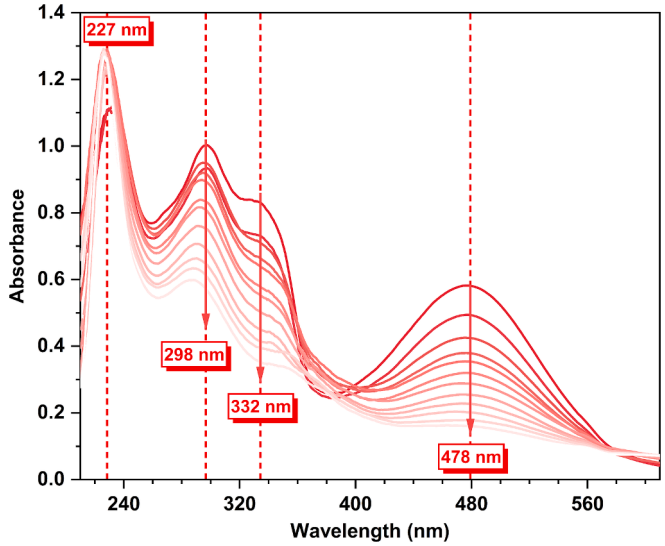

Fig. 3. Absorption spectral titration of *in-situ* prepared **$CuCl_2L$** receptor (38 μM, 1.7 mL) upon gradual addition of S^{2-} (Na_2S 0.1 mM, 4 μL) in aqueous acetonitrile (2:1 v/v, 10 mM HEPES, pH 7.4). Arrows indicate the effect of the gradual addition of sulfide on the absorption spectrum.

332 nm, and notably in the 478 nm band, which almost vanished upon reaching saturation with the added aqueous sulfide species (totaling up to 40 μL, 0.1 mM).

This experiment revealed that the addition of nearly 0.1 equivalent of Na_2S was sufficient to displace the Cu(II) ion from the **$CuCl_2L$** receptor. The receptor's absorption spectrum showed significant sensitivity to even minor variations in sulfide concentration, indicating its high efficacy in detecting the presence of sulfide species. Through this analysis, the detection limit [97,98] of the **$CuCl_2L$** receptor for sulfide was determined as 82.50 nM, underscoring its potential as a sensitive tool for sulfide detection.

The selective sensing capability of the **$CuCl_2L$** receptor for sulfide species was further validated through a competition experiment. In this experiment, aqueous solutions of various anions, each at a higher concentration (ten equivalents) including F^-, Cl^-, Br^-, I^-, $CH_3CO_2^-$, HCO_3^-, $H_2PO_4^-$, NO_3^-, SO_3^{2-}, SO_4^{2-}, $S_2O_3^{2-}$, CO_3^{2-}, and HPO_4^{2-} (10 mM, 57 μL), were individually added to the **$CuCl_2L$** receptor solution (38 μM, 1.5 mL). Subsequently, one equivalent of S^{2-} (Na_2S 1 mM, 57 μL) was introduced into each mixture.

Initially, the presence of ten equivalents of other anions (excluding Na_2S) did not significantly impact the absorption spectrum of the **$CuCl_2L$** receptor. However, upon the addition of one equivalent of Na_2S, there was a notable alteration in the receptor's absorption spectrum. This was marked by the near disappearance of the 478 nm absorption band, leading the spectrum to resemble that of the free ligand **L**, as shown in Fig. 4.

Furthermore, when a mixture containing ten equivalents of all the aforementioned anions (except Na_2S) was added to the **$CuCl_2L$** receptor, followed by the introduction of one equivalent of the sulfide anion, similar results were observed. This outcome from the competition experiments decisively confirms the receptor's ability to selectively recognize sulfide, even in the presence of a mixture of other anions at concentrations ten times higher.

The conditions for sulfide detection established in our study not only align well with those reported in existing literature but also demonstrate a notably improved detection limit and response time compared to the majority of previously documented receptor systems. These enhancements are clearly evidenced in our comprehensive comparison, as summarized in Table 1, emphasizing the advanced efficiency and sensitivity of our receptor system in sulfide sensing applications.

3.2. *Real-time applications of sulfide detection*

3.2.1. *Effect of pH variation and water tolerance on the in-situ prepared $CuCl_2L$ receptor for sulfide detection*

We conducted a thorough analysis of the *in-situ* prepared **$CuCl_2L$** receptor's response to pH variations in relation to sulfide detection. Utilizing UV–Vis absorption spectroscopy, the receptor's behavior was monitored across a pH range of 1 to 12 in an aqueous acetonitrile solution (2:1 v/v, 10 mM HEPES). The findings reveal that the **$CuCl_2L$** receptor maintains stability within the pH range of 4 to 9 and is, therefore, most effective for sulfide detection under these conditions (see Fig. 5). Outside this range, the receptor undergoes hydrolysis, regenerating the free ligand **L**, which compromises its functionality.

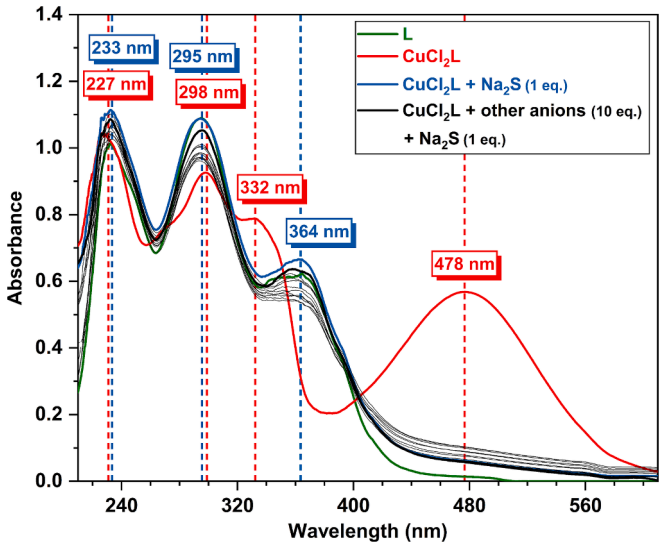

Fig. 4. Absorption spectra of *in-situ* prepared **$CuCl_2L$** receptor (38 μM, 1.5 mL) upon addition of different anions (F^-, Cl^-, Br^-, I^-, $CH_3CO_2^-$, HCO_3^-, $H_2PO_4^-$, NO_3^-, SO_3^{2-}, SO_4^{2-}, $S_2O_3^{2-}$, CO_3^{2-}, and HPO_4^{2-}) (10 mM, 57 μL) followed by S^{2-} (Na_2S 1 mM, 57 μL) addition in aqueous acetonitrile (2:1 v/v, 10 mM HEPES, pH 7.4).

Table 1
Important analytical parameters of a few reported receptors for sulfide sensing.

Probe	Receptor Probe	Detection Conditions/ Medium	Detection Limit (approximate)	Response Time (approximate)	Ref.
01	Benzimidazole-based benzoate Cu(II) receptor	HEPES buffer (20 mM, pH 7.4)	2.51 μM	–	[9]
02	2-methylquinoline-based benzohydrazide Cu(II) receptor	DMSO/HEPES (9:1 v/v, 20 mM, pH 7.22)	0.949 μM		[12]
03	Azo-dye-based bis-Schiff based receptor	DMF/ H_2O (1:1 v/v, 10 mM, pH 7.4)	1.7 μM 0.335 μM	<10 s	[14]
04	Imidazole-based Cu(II) receptor	Isopropanol/H_2O (1:1 v/v, *Bis-Tris buffer,* pH 7)	1.2 μM	–	[28]
05	Benzimidazole-based Cu(II) receptor	HEPES buffer (20 mM, pH 6.0)	1.35 μM	30 s	[29]
06	Pyridoxal Schiff base-based Cu(II) receptors	MeOH/H_2O	3.4 μM 3.2 μM	–	[34]
07	Quinoline-pyrazoline based Cu(II) receptor	DMSO/PBS buffer (1:9 v/v, pH 7.4)	0.2 μM	–	[36]
08	Coumarin–dipicolylamine-based Cu(II) receptor	CH_3CN/HEPES buffer (1:19 v/v, 10 mM, pH 7.4)	14 nM	Few seconds	[43]
09	Schiff-base-based receptor	DMSO/bis-Tris buffer (9:1 v/v)	4.0 μM	Few seconds	[48]
10	Terephthalic acid-coordinated Cu(II) MOF	H_2O	10.0 μM	20 min	[66]
11	Silver nanoparticles capped with carbon dots (AgNPs-CDs)	H_2O	0.01 μM	–	[67]
12	Peptide-based Hg(II) receptor	HEPES buffer (10 mM, pH 7.4)	60.9 nM	40 s	[99]
13	Silver/nitrogen-doped carbon nanoparticles (Ag/NCNPs)	H_2O	0.18 μM	1 min	[100]
14	Cyclam-functionalized carbon dot-based Cu(II) receptor	HEPES buffer (pH 7.4)	0.13 μM	–	[101]
15	Quinolimide-based Cu(II) receptor	CH_3CN/H_2O (1:1 v/v, pH 7.2)	0.178 μM	0.5 min	[102]
16	Peptide-based Cu(II) and Hg(II) receptor	HEPES buffer (10 mM, pH 7.4)	0.27 μM and 0.12 μM	50 s	[103]
17	dppy-based Cu(II) receptor (**$CuCl_2L$**)	CH_3CN/HEPES buffer (1:2 v/v, 10 mM, pH 7.4)	82.50 nM	Immediate	**Present Work**

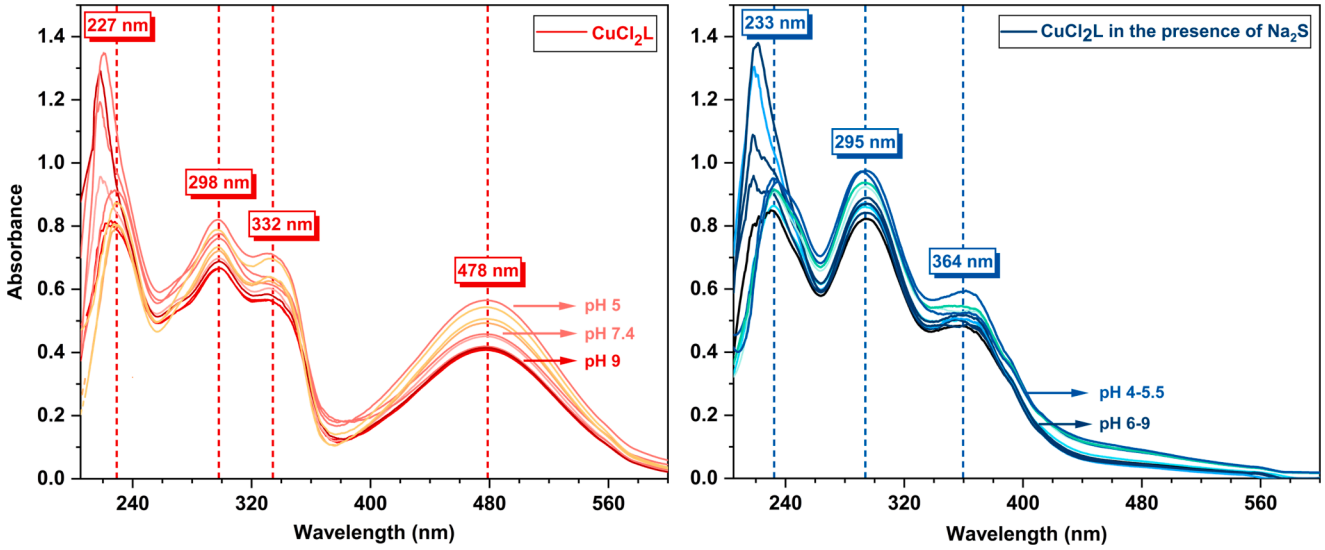

Fig. 5. UV–Vis absorption spectra of (left) *in-situ* prepared **$CuCl_2L$** (38 μM, 1.5 mL) and (right) *in-situ* prepared **$CuCl_2L$** (38 μM, 1.5 mL) with S^{2-} (Na_2S, 1 eq., 1 mM, 57 μL) in aqueous acetonitrile (2:1 v/v, 10 mM HEPES, $4 \leq pH \leq 9$).

The ligand **L** is highly soluble in acetonitrile but insoluble in water, leading to precipitation as the water content in the acetonitrile solution increases. However, in aqueous acetonitrile (2:1 v/v) within the optimal pH range of 4 to 9, the *in-situ* prepared **$CuCl_2L$** receptor exhibited good water tolerance and retained its effectiveness for sulfide detection. Upon the introduction of sulfide ions in solutions with higher water content, Cu(II) was displaced from the **$CuCl_2L$** complex, leading to the formation of CuS, but this also caused the precipitation of **L** due to its insolubility. This precipitation interfered with the absorption spectra. To minimize this interference and maintain clear spectral readings, we recommend using a 2:1 (v/v) water-to-acetonitrile ratio.

3.2.2. *Naked eye colorimetric test using glass vials*

For a naked-eye colorimetric test, we added one equivalent of S^{2-} (Na_2S 1 mM, 57 μL) and ten equivalents of other anions (10 mM, 57 μL) to separate glass vials containing the *in-situ* prepared **$CuCl_2L$** receptor (38 μM, 1.5 mL) in aqueous acetonitrile (2:1 v/v, 10 mM HEPES, pH 7.4), as depicted in Fig. 6. Notably, the addition of just one equivalent of Na_2S to the light brownish-red colored **$CuCl_2L$** receptor solution resulted in an immediate color change to almost colorless, mirroring the colorless nature of **L** in acetonitrile. Conversely, the addition of other anions (ten equivalents) did not induce any color change in the **$CuCl_2L$** receptor solution. This stark contrast in color response distinctly highlights the **$CuCl_2L$** receptor's exceptional capability for naked-eye colorimetric detection of sulfide in an aqueous acetonitrile medium. Furthermore, for colorimetric detection, a higher water content than the recommended 2:1 (v/v) water-to-acetonitrile ratio can be used without compromising the detection capability. In this case, the **$CuCl_2L$** receptor remains

Fig. 6. Colorimetric picture of the *in-situ* prepared **$CuCl_2L$** (38 μM, 1.5 mL) upon addition of S^{2-} (Na_2S 1 mM, 57 μL) and 10 equivalents of different anions (F^-, Cl^-, Br^-, I^-, $CH_3CO_2^-$, HCO_3^-, $H_2PO_4^-$, NO_3^-, SO_3^{2-}, SO_4^{2-}, $S_2O_3^{2-}$, CO_3^{2-}, and HPO_4^{2-}; 10 mM, 57 μL) in aqueous acetonitrile (2:1 v/v, 10 mM HEPES, pH 7.4).

effective for sulfide detection, even with the additional precipitation of **L**.

3.2.3. Spray test on tissue papers

A spray test on tissue papers was conducted to demonstrate the practical application of the **$CuCl_2L$** receptor in sulfide detection. In this experiment, one equivalent of Na_2S (1 mM), ten equivalents of various other anions (10 mM), and the *in-situ* prepared **$CuCl_2L$** receptor (38 μM) were used in an aqueous acetonitrile solution (2:1 v/v, 10 mM HEPES, pH 7.4).

Initially, tissue papers were immersed in different analyte solutions and dried. These papers were then sprayed with the **$CuCl_2L$** receptor solution (Fig. 7a). In a complementary approach, other tissue papers were first soaked with the in-situ prepared **$CuCl_2L$** receptor, dried, and then sprayed with solutions of different analytes (Fig. 7b).

In both experimental setups, the results were consistent with those obtained from the naked-eye colorimetric tests in glass vials. The application of the **$CuCl_2L$** receptor, whether sprayed onto the analyte-soaked papers or used as a spray on receptor-soaked papers, led to an immediate and discernible color change. This change was a clear indicator of the presence of sulfide, demonstrating the receptor's capability for effective and low-cost nanomolar-level sulfide detection. The simplicity and rapid response of this method hold great promise for practical applications in sulfide monitoring.

3.2.4. Sulfide detection in various water samples

Next, we conducted sulfide estimation experiments on a diverse range of water samples, including river, pond, tap, and supply water, using our *in-situ* prepared **$CuCl_2L$** receptor (38 μM). The findings, detailed in Table 2, demonstrate that the sulfide detection efficacy of the **$CuCl_2L$** receptor is on par with previously reported receptors [100]. This suggests its potential for broad application in analyzing various types of water samples.

3.2.5. DNA binding study

Anti-cancer drugs function by binding to DNA, altering the DNA replication process, thereby inhibiting the growth of cancer cells and inducing apoptosis [41,104]. In this context, copper complexes have garnered significant interest due to their unique non-covalent DNA binding interactions and mechanisms of action, which differ markedly from those of platinum complexes [39,105]. To evaluate the DNA-binding capability of our *in-situ* synthesized **$CuCl_2L$** receptor, we conducted absorption and emission spectral titrations. These experiments were performed in an aqueous acetonitrile HEPES buffer at a pH of 7.4.

In our UV–Vis absorption spectral studies, **(**Fig 8a**)** the *in-situ* prepared **$CuCl_2L$** receptor exhibited notable changes upon the gradual addition of DNA. Specifically, the characteristic LMCT absorption band at 478 nm displayed hypochromic shifts and a significant bathochromic shift of approximately 33 nm. This observation suggests a strong non-covalent intercalative binding, characterized by the stacking interaction between the planar aromatic chromophore of the **$CuCl_2L$** receptor and DNA base pairs [73,106]. This binding mechanism is further substantiated by a high intrinsic binding constant, $K_b = 7.74 \times 10^5\ M^{-1}$, calculated through application of equation (1). A plot of $[\text{CT-DNA}]/(\varepsilon_a - \varepsilon_f)$ versus [CT-DNA] is shown in Fig. S11a.

Additionally, this absorption spectral study is corroborated by the EB displacement assay in our emission spectral study **(**Fig 8b**)**. The gradual addition of the **$CuCl_2L$** receptor (90 μM, 50 μL, non-fluorescent**)** to the fluorescent EB-CT-DNA adduct (40 μM, 1.8 mL) resulted in steady hypochromic shifts in the emission band of the adduct, indicative of intercalation by the **$CuCl_2L$** receptor [70,107]. The robustness of this intercalative binding interaction is further evidenced by the high values of $K_{app} = 2.381 \times 10^7\ M^{-1}$ and $K_{SV} = 7.065 \times 10^4\ M^{-1}$, calculated using equations (3) and (2), respectively, from the linear fit plot of F_0/F vs **[$CuCl_2L$]** (μM) (see Fig. S11b).

Further elucidation of the binding interactions between the **$CuCl_2L$** receptor and CT-DNA were observed through a viscometry titration experiment. This study revealed that the specific viscosity of CT-DNA (10 mM HEPES, pH 7.4) gradually increased upon gradual addition of

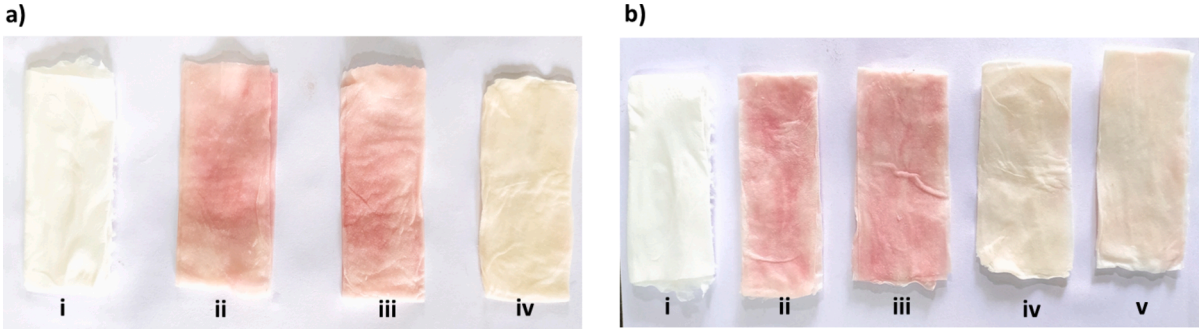

Fig. 7. a) Tissue papers initially immersed in various analyte solutions and dried, followed by treatment with the **$CuCl_2L$** receptor solution by spraying. i) Fresh tissue paper; ii) no analytes; iii) mixture of other anions (except Na_2S), iv) mixture of other anions and Na_2S. **b)** Tissue papers pre-treated with the *in-situ* prepared **$CuCl_2L$** receptor (38 μM), followed by spraying with solutions of different analytes. i) Fresh tissue paper; ii) no analytes, iii) mixture of other anions (excluding Na_2S), iv) Na_2S, v) mixture of other anions including S^{2-} (Na_2S).

Table 2
Estimation of sulfide concentration in various water samples.

Water Sample	Added (μM)	Found (μM)	Recovery (%)	Water Sample	Added (μM)	Found (μM)	Recovery (%)
Supply water	2	1.88	94.00	Lab water	2	1.80	90.00
	4	3.77	94.25		4	3.61	90.25
	6	5.66	94.33		6	5.37	89.50
Pond water	2	2.17	108.50	River water	2	2.16	108.00
	4	4.11	102.75		4	4.10	102.50
	6	5.89	98.17		6	5.93	98.83

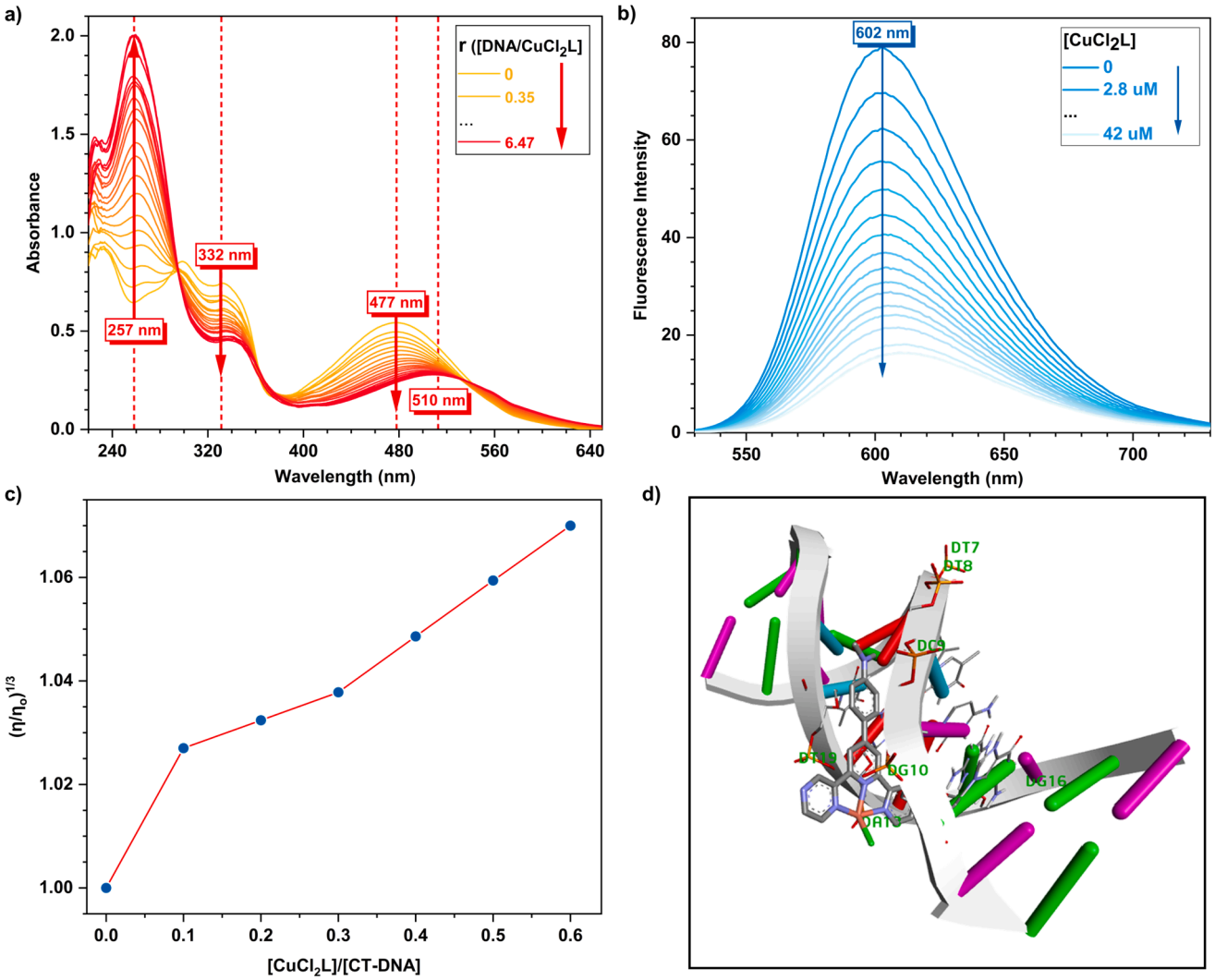

Fig. 8.A. **a)** Absorption spectra of the *in-situ* prepared **$CuCl_2L$** receptor (32 μM, 1.5 mL) upon gradual addition of CT-DNA (15 μL) in aqueous acetonitrile (2:1 v/v, 10 mM HEPES, pH 7.4). **b)** Emission spectra of EB-CT-DNA (40 μM, 1.8 mL) in aqueous HEPES buffer (10 mM, pH 7.4) upon gradual addition of *in-situ* prepared **$CuCl_2L$** receptor (90 μM, 50 μL). **c)** Effect of the **$CuCl_2L$** receptor addition on the relative viscosity of CT-DNA. **d)** Molecular docking model of the **$CuCl_2L$** receptor's interaction with CT-DNA (PDB ID: 1BNA).

$CuCl_2L$ receptor. This increase is attributed to the intercalation of **$CuCl_2L$** receptor into the CT-DNA, leading to an elongation of its double helix structure, and, consequently, an increase in specific viscosity. This observation strongly supports the hypothesis of intercalative binding between the **$CuCl_2L$** receptor and CT-DNA. The specific viscosity values of CT-DNA were derived from the $(\eta/\eta_0)^{1/3}$ vs [**$CuCl_2L$**/CT-DNA] plot (Fig 8c) [108,109].

Finally, a molecular docking study was also carried out to investigate the mechanism of the binding interactions of the **$CuCl_2L$** receptor with CT-DNA. The lowest-energy structure obtained from this investigation (Fig 8d) revealed that the **$CuCl_2L$** receptor binds to a minor groove of DNA. This binding is characterized by multiple interactions: strong conventional N–H bonding between a free N atom of one of the pyrazine moieties of the receptor and nucleobase DG 16 (2.40 Å); strong C–H bonding between the C atom of the amine moiety (NMe_2) with nucleobases DT 19 (2.93 Å) and DT 7 (3.08 Å); C–H bonding between the C atom of a pyrazine moiety with nucleobase DC 9 (3.28 Å); and weak π–alkyl interaction between the methyl groups of the receptor's amino moiety and the aromatic π-electron cloud of nucleobases DA 18 (5.29 Å), DT 8 (5.28 Å), and DT 19 (5.17 Å). Additionally, a strong π−anion interaction was observed between the π-electron cloud of a pyrazine moiety of the **$CuCl_2L$** and the phosphate anion of DG 10 (3.36 Å),

indicating strong intercalative binding. A 3-D graphical representation depicting the CT-DNA binding interaction of the $CuCl_2L$ receptor, illustrating both the hydrogen bonding and π-stacking interactions, is shown in Fig. S14. These molecular docking findings align well with the results obtained from our absorption, emission spectral studies, and viscometry titrations, thereby corroborating the **$CuCl_2L$** receptor's intercalative binding mechanism with CT-DNA.

3.2.6. *BSA binding interaction study*

In the absorption spectral experiment, the gradual addition of the *in-situ* prepared **$CuCl_2L$** receptor to BSA (in a 100 mM PB buffer, 2 mL) led to the emergence of a new absorption band at 460 nm. This band displayed a consistent hyperchromic shift, indicating a binding interaction between the **$CuCl_2L$** receptor and BSA (Fig 9a**)**. Additionally, in our emission spectral study, which focused on tryptophan quenching in BSA, a gradual decrease in the intrinsic fluorescence intensity of BSA was observed (evidenced by a hypochromic shift) with the increasing concentration of the *in-situ* prepared **$CuCl_2L$** receptor (Fig 9b**)** [110]. This quenching effect suggests a conformational change in BSA's hydrophobic cavity, particularly in the subdomain IIA containing the Trp-214 residue [111], caused by the receptor binding to BSA. This hypothesis is further supported by a comparatively high dynamic quenching constant, $K_{SV} = 1.6 \times 10^5\ M^{-1}$, calculated from the linear fit plot of F_0/F vs [**$CuCl_2L$**] (equation (2), see Fig. S12a). Moreover, the binding stoichiometry, approximately $n \sim 1$ (0.82), suggests a 1:1 binding ratio of the **$CuCl_2L$** receptor to BSA. The affinity constant, $K = 2.158 \times 10^4\ M^{-1}$, calculated from the linear fit plot of $\log(F_0 - F)/F$ vs $\log$[**$CuCl_2L$**] (equation (4), see Fig. S12b) reinforces the binding affinity of the **$CuCl_2L$** receptor to BSA.

The molecular docking study also revealed that **$CuCl_2L$** receptor interacts with BSA, exhibiting a binding energy of –5.99 kcal mol^{-1}. The major interactions of the **$CuCl_2L$** receptor with the protein include a conventional hydrogen bond between the free N atom of one of its pyrazine moieties and ARG427 (2.20 Å), this pyrazine moiety also engaging in a π–alkyl interaction with ARG427 (5.41 Å). In turn, the other pyrazine moiety engages in a π–cation interaction with HIS145 (4.83 Å) and ARG458 (4.19 Å). Additionally, the pyridine moiety of the **$CuCl_2L$** receptor is involved in π–anion interaction with the GLU424 (3.38 Å). The benzene ring of the receptor exhibits π–alkyl interactions with ALA193 (4.65 Å) and ILE455 (5.48 Å). Furthermore, two alkyl moieties of the receptor's amine group form π–alkyl interaction with TYR451 (4.32 Å and 4.84 Å). These diverse N–H bonding, π–cation, π–anion, and π–alkyl interactions collectively stabilize the **$CuCl_2L$** receptor within the hydrophobic cavity of BSA. A 3-D graphical representation depicting the BSA binding interaction of the **$CuCl_2L$** receptor in more detail is shown in Fig. S15. The molecular docking results corroborate the binding study findings of the **$CuCl_2L$** receptor with BSA, as observed in the UV–Vis absorption and fluorescence emission spectral studies. Details of the binding energy of various conformations of the BSA-**$CuCl_2L$** receptor and active L-amino acids residues nearby the **$CuCl_2L$** receptor are provided in Table S3.

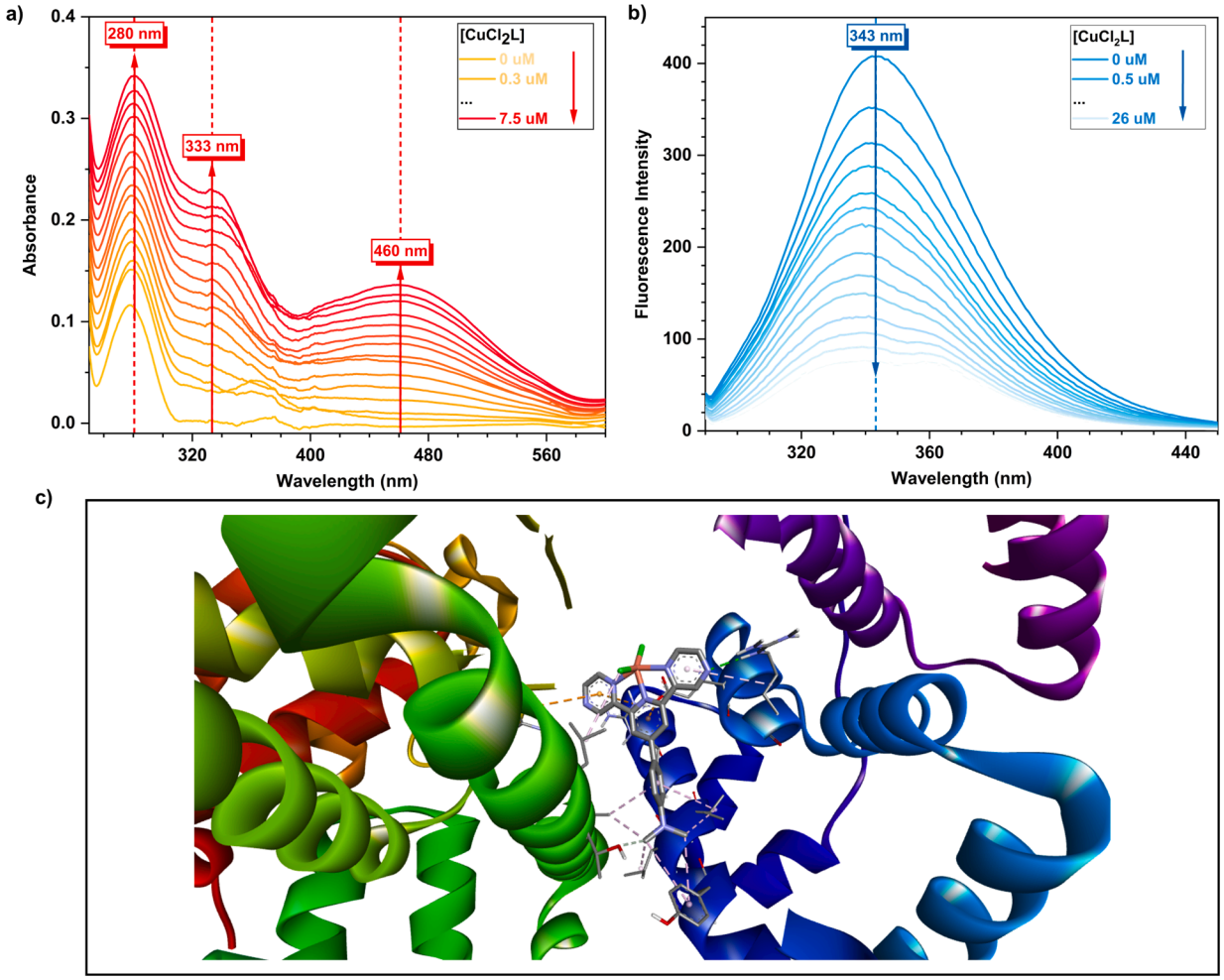

Fig. 9.A. a) Absorption and **b)** emission spectra of gradual addition of the *in-situ* prepared **$CuCl_2L$** receptor to a BSA solution in aqueous PB buffer (10 mM HEPES, pH 7.4). **c)** Molecular docking model of the **$CuCl_2L$** receptor's interaction with BSA (PDB ID: 4F5S).

4. Conclusions

In summary, recognizing the critical need for sulfide detection from biological, chemical, and environmental perspectives, we have developed and characterized a simple Cu(II)-dppy complex, **$CuCl_2$L**. This complex is a 1:1 Cu(II) coordination of 4-(2,6-di(pyrazin-2-yl)pyridin-4-yl)-*N*,*N*-dimethylaniline ligand **L**, whose properties were elucidated through a combination of spectroscopic techniques, including UV–Vis, FT-IR, HRMS, elemental analysis, and ESR, alongside quantum chemical calculations at the DFT and TD-DFT levels. UV–Vis absorption spectral studies confirmed the capability of the *in-situ* prepared **$CuCl_2$L** receptor to selectively detect sulfide at nanomolar levels, even in the presence of a tenfold excess of various other anions, namely F^-, Cl^-, Br^-, I^-, $CH_3CO_2^-$, HCO_3^-, $H_2PO_4^-$, NO_3^-, SO_3^{2-}, SO_4^{2-}, $S_2O_3^{2-}$, CO_3^{2-}, and HPO_4^{2-}, in aqueous acetonitrile (2:1 v/v, 10 mM HEPES, pH 7.4). The receptor exhibited an impressive detection limit of 82.50 nM. Additionally, the *in-situ* prepared **$CuCl_2$L** receptor presented a cost-effective approach for various real-time applications in sulfide anion detection. Further studies, including absorption, emission spectral analysis, viscometry, and molecular docking, have substantiated the **$CuCl_2$L** receptor's significant intercalative binding interaction with CT-DNA (binding constants: $K_b = 7.74 \times 10^5\ M^{-1}$, $K_{app} = 2.381 \times 10^7\ M^{-1}$ and $K_{SV} = 7.065 \times 10^4\ M^{-1}$) and its effective binding interactions with BSA (binding constants, $K_{ab} = 2.158 \times 10^4\ M^{-1}$ and $K_{SV} = 1.6 \times 10^5\ M^{-1}$).

CRediT authorship contribution statement

Dipankar Das: Writing – original draft, Visualization, Methodology, Investigation, Formal analysis, Conceptualization. **Aritra Roy:** Software, Investigation, Formal analysis. **Cauê P. Souza:** Supervision, Investigation, Formal analysis. **Somnath Mondal:** Methodology, Formal analysis. **Sourav Sutradhar:** Software, Formal analysis. **Parnashabari Sarkar:** Software, Investigation, Formal analysis. **Felipe Fantuzzi:** Writing – original draft, Supervision, Software, Funding acquisition, Conceptualization. **Biswa Nath Ghosh:** Writing – review & editing, Visualization, Supervision, Funding acquisition, Conceptualization.

Declaration of competing interest

The authors declare that they have no known competing financial interests or personal relationships that could have appeared to influence the work reported in this paper.

Acknowledgements

D.D. acknowledges NIT Silchar for financial support. This work was supported by the Engineering and Physical Sciences Research Council [grant number EP/W52461X/1]. This article is also based upon work from the COST Action CA20129 - Multiscale Irradiation and Chemistry Driven Processes and Related Technologies (MultIChem), supported by COST (European Cooperation in Science and Technology). C.P.S. and F. F. acknowledge the University of Kent for financial and computational support. Special thanks are extended to Dr Timothy Kinnear for HPC assistance.

Appendix A. Supplementary data

Supplementary data to this article can be found online at https://doi.org/10.1016/j.jphotochem.2024.116154.

Data availability

Data will be made available on request.

References

[1] C. Kar, M.D. Adhikari, A. Ramesh, G. Das, NIR-and FRET-based sensing of Cu^{2+} and S^{2-} in physiological conditions and in live cells, Inorg. Chem. 52 (2013) 743–752, https://doi.org/10.1021/ic301872q.
[2] Y. Hu, J. Yin, J. Yoon, A multi-responsive cyanine-based colorimetric chemosensor containing dipicolylamine moieties for the detection of Zn(II) and Cu(II) ions, Sens. Actuators B Chem. 230 (2016) 40–45, https://doi.org/10.1016/j.snb.2016.02.040.
[3] C. Kar, G. Das, A retrievable fluorescence "TURN ON" sensor for sulfide anions, J. Photochem. Photobiol. A Chem. 251 (2013) 128–133, https://doi.org/10.1016/j.jphotochem.2012.10.024.
[4] S. Wang, L. Gong, G. El Fakhri, J. Wang, Efficient synthesis of 6,6′-diamido-2,2′-dipicolylamine ligands for potential phosphate anion sensing, New J. Chem. 45 (2021) 16833–16840, https://doi.org/10.1039/d1nj03030b.
[5] M. Shakir, A. Abbasi, Solvent dependant isatin-based Schiff base sensor as fluorescent switch for detection of Cu^{2+} and S^{2-} in human blood serum, Inorganica Chim. Acta. 465 (2017) 14–25, https://doi.org/10.1016/j.ica.2017.04.057.
[6] P. Nagy, Z. Pálinkás, A. Nagy, B. Budai, I. Tóth, A. Vasas, Chemical aspects of hydrogen sulfide measurements in physiological samples, Biochim. Biophys. Acta Gen. Subj. 1840 (2014) 876–891, https://doi.org/10.1016/j.bbagen.2013.05.037.
[7] Y. Sun, J.A.R. Soedarso, J. Wang, P. Gremmen, H. Rijnaarts, W. Chen, Use of ion chromatographic pulsed amperometric method (IC-PAD) for measuring aqueous sulfide in synthetic and real domestic wastewater, Chemosphere 313 (2023) 137442, https://doi.org/10.1016/j.chemosphere.2022.137442.
[8] A.K. Mahapatra, S. Mondal, S.K. Manna, K. Maiti, R. Maji, M.R. Uddin, S. Mandal, D. Sarkar, T.K. Mondal, D.K. Maiti, A new selective chromogenic and turn-on fluorogenic probe for copper(II) in solution and vero cells: Recognition of sulphide by [CuL], Dalton Trans. 44 (2015) 6490–6501, https://doi.org/10.1039/c4dt03969f.
[9] Y. Fu, Q.C. Feng, X.J. Jiang, H. Xu, M. Li, S.Q. Zang, New fluorescent sensor for Cu^{2+} and S^{2-} in 100% aqueous solution based on displacement approach, Dalton Trans. 43 (2014) 5815–5822, https://doi.org/10.1039/c3dt53281j.
[10] A.H. Gore, S.B. Vatre, P.V. Anbhule, S.H. Han, S.R. Patil, G.B. Kolekar, Direct detection of sulfide ions [S^{2-}] in aqueous media based on fluorescence quenching of functionalized CdS QDs at trace levels: Analytical applications to environmental analysis, Analyst 138 (2013) 1329–1333, https://doi.org/10.1039/c3an36825d.
[11] Y. Wang, H. Sun, L. Hou, Z. Shang, Z. Dong, W. Jin, 1,4-Dihydroxyanthraquinone-Cu^{2+} ensemble probe for selective detection of sulfide anion in aqueous solution, Anal. Methods 5 (2013) 5493–5500, https://doi.org/10.1039/c3ay40977e.
[12] C. Gao, X. Liu, X. Jin, J. Wu, Y. Xie, W. Liu, X. Yao, Y. Tang, A retrievable and highly selective fluorescent sensor for detecting copper and sulfide, Sens. Actuators B Chem. 185 (2013) 125–131, https://doi.org/10.1016/j.snb.2013.04.110.
[13] F. Hou, L. Huang, P. Xi, J. Cheng, X. Zhao, G. Xie, Y. Shi, F. Cheng, X. Yao, D. Bai, Z. Zeng, A retrievable and highly selective fluorescent probe for monitoring sulfide and imaging in living cells, Inorg. Chem. 51 (2012) 2454–2460, https://doi.org/10.1021/ic2024082.
[14] A.K. Manna, J. Mondal, R. Chandra, K. Rout, G.K. Patra, A fluorescent colorimetric: Azo dye based chemosensor for detection of S^{2-} in perfect aqueous solution and its application in real sample analysis and building a molecular logic gate, Anal. Methods 10 (2018) 2317–2326, https://doi.org/10.1039/c8ay00470f.
[15] P.M. May, D. Batka, G. Hefter, E. Königsberger, D. Rowland, Goodbye to S^{2-} in Aqueous Solution, Chem. Commun. 54 (2018) 1980–1983, https://doi.org/10.1039/C8CC00187A.
[16] M. Queizán, A.M. Graña, J.M. Hermida-ramón, Achieving S^{2-} in aqueous Solution : An evaluation using First-Principle molecular dynamics simulations, J. Mol. Liq. 349 (2022) 118109, https://doi.org/10.1016/j.molliq.2021.118109.
[17] Z.L. Song, L. Zhao, T. Ma, Progress and perspective on hydrogen sulfide donors and their biomedical applications, Med. Res. Rev. 42 (2022) 1930–1977, https://doi.org/10.1002/med.21913.
[18] G. Yang, L. Wu, B. Jiang, W. Yang, J. Qi, K. Cao, Q. Meng, A.K. Mustafa, W. Mu, S. Zhang, S.H. Snyder, R. Wang, H_2S as a Physiologic Vasorelaxant: Hypertension in Mice with Deletion of Cystathionine γ-Lyase, Science 322 (2008) 587–590, https://doi.org/10.1126/science.1162667.
[19] K. Abe, H. Kimura, The possible role of hydrogen sulfide as an endogenous neuromodulator, J. Neurosci. 16 (1996) 1066–1071, https://doi.org/10.1523/JNEUROSCI.16-03-01066.1996.
[20] J.L. Wallace, J.G.P. Ferraz, M.N. Muscara, Hydrogen Sulfide : an Endogenous Mediator of Resolution of Inflammation and Injury, Antioxid. Redox Signal. 17 (2012) 58–67, https://doi.org/10.1089/ars.2011.4351.
[21] W. Han, Z. Dong, C. Dimitropoulou, Y. Su, Hydrogen Sulfide Ameliorates Tobacco Smoke-Induced Oxidative Stress and Emphysema in Mice, Antioxid. Redox Signal. 15 (2011) 2121–2134, https://doi.org/10.1089/ars.2010.3821.
[22] J.W. Elrod, J.W. Calvert, J. Morrison, J.E. Doeller, D.W. Kraus, L. Tao, X. Jiao, R. Scalia, L. Kiss, C. Szabo, H. Kimura, C. Chow, D.J. Lefer, Hydrogen sulfide attenuates myocardial ischemia-reperfusion injury by preservation of mitochondrial function, Proc. Natl. Acad. Sci. 104 (2007) 15560–15565, https://doi.org/10.1073/pnas.0705891104.
[23] B. Pomierny, W. Krzy, J. Jurczyk, A. Sk, B. Strach, M. Szafarz, K. Przejczowska-pomierny, R. Torregrossa, M. Whiteman, M. Marcinkowska, J. Pera, B. Budziszewska, The Slow-Releasing and Mitochondria-Targeted Hydrogen

Sulfide (H_2S) Delivery Molecule AP39 Induces Brain Tolerance to Ischemia, Int. J. Mol. Sci. 22 (2021) 7816, https://doi.org/10.3390/ijms22157816.
[24] U. Shefa, M. Kim, N.Y. Jeong, J. Jung, Antioxidant and Cell-Signaling Functions of Hydrogen Sulfide in the Central Nervous System, Oxid. Med. Cell. Longev. 2018 (2018) 1873962, https://doi.org/10.1155/2018/1873962.
[25] Y. Zhao, M.D. Pluth, Hydrogen Sulfide Donors Activated by Reactive Oxygen Species, Angew. Chem. Int. Ed. 55 (2016) 14638–14642, https://doi.org/10.1002/anie.201608052.
[26] J. Ge, Y. Shen, W. Wang, Y. Li, Y. Yang, N-doped carbon dots for highly sensitive and selective sensing of copper ion and sulfide anion in lake water, J. Environ. Chem. Eng. 9 (2021) 105081, https://doi.org/10.1016/j.jece.2021.105081.
[27] K. Eto, T. Asada, K. Arima, T. Makifuchi, H. Kimura, Brain hydrogen sulfide is severely decreased in Alzheimer's disease, Biochem. Biophys. Res. Commun. 293 (2002) 1485–1488, https://doi.org/10.1016/S0006-291X(02)00422-9.
[28] M.H. Mahnashi, A.M. Mahmoud, S.A. Alkahtani, R. Ali, M.M. El-Wekil, A novel imidazole derived colorimetric and fluorometric chemosensor for bifunctional detection of copper (II) and sulphide ions in environmental water samples, Spectrochim. Acta A Mol. Biomol. Spectrosc. 228 (2020) 117846, https://doi.org/10.1016/j.saa.2019.117846.
[29] L. Tang, M. Cai, Z. Huang, K. Zhong, S. Hou, Y. Bian, R. Nandhakumar, Rapid and highly selective relay recognition of Cu(II) and sulfide ions by a simple benzimidazole-based fluorescent sensor in water, Sens. Actuators B Chem. 185 (2013) 188–194, https://doi.org/10.1016/j.snb.2013.04.109.
[30] X. Cao, W. Lin, L. He, A near-infrared fluorescence turn-on sensor for sulfide anions, Org. Lett. 13 (2011) 4716–4719, https://doi.org/10.1021/ol201932c.
[31] F. Zheng, M. Wen, F. Zeng, S. Wu, A robust, water-soluble and low cytotoxic fluorescent probe for sulfide anion achieved through incorporation of betaine, Sens. Actuators B Chem. 188 (2013) 1012–1018, https://doi.org/10.1016/j.snb.2013.08.003.
[32] R. Kaushik, A. Ghosh, D. Amilan Jose, Recent progress in hydrogen sulphide (H_2S) sensors by metal displacement approach, Coord. Chem. Rev. 347 (2017) 141–157, https://doi.org/10.1016/j.ccr.2017.07.003.
[33] M. Colon, J.L. Todolí, M. Hidalgo, M. Iglesias, Development of novel and sensitive methods for the determination of sulfide in aqueous samples by hydrogen sulfide generation-inductively coupled plasma-atomic emission spectroscopy, Anal. Chim. Acta 609 (2008) 160–168, https://doi.org/10.1016/j.aca.2008.01.001.
[34] M. Chakraborty, A. Mondal, S.K. Chattopadhyay, Structural divergence in binuclear Cu(II) pyridoxal Schiff base complexes probed by co-ligands: Catecholase mimetic activity and sulphide ion sensing, New J. Chem. 44 (2020) 12916–12925, https://doi.org/10.1039/d0nj00719f.
[35] J. Park, T. Kang, S. Jin, Y. Heo, K. Kim, K. Lee, P. Tsai, C. Yoon, Asphyxiation Incidents by Hydrogen Sulfide at Manure Storage Facilities of Swine Livestock Farms in Korea, J. Agromedicine 21 (2016) 114–148, https://doi.org/10.1080/1059924X.2016.1141735.
[36] G. Subashini, A. Saravanan, S. Shyamsivappan, T. Arasakumar, V. Mahalingam, R. Shankar, P.S. Mohan, A versatile "on-off-on" quinoline pyrazoline hybrid for sequential detection of Cu^{2+} and S^{-} ions towards bio imaging and tannery effluent monitoring, Inorg. Chim. Acta 483 (2018) 173–179, https://doi.org/10.1016/j.ica.2018.08.012.
[37] Q. Zhao, Z. Tang, Y. Pan, J. Han, J. Yang, The Ksp gap enabled precipitation transformation reactions from transition metal hydroxides to sulfides for alkali metal ion storage, Inorg. Chem. Front. 10 (2023) 3406–3414, https://doi.org/10.1039/d3qi00324h.
[38] H. Fang, P.C. Huang, F.Y. Wu, A novel jointly colorimetric and fluorescent sensor for Cu2+ recognition and its complex for sensing S^{2-} by a Cu^{2+} displacement approach in aqueous media, Spectrochim. Acta A Mol. Biomol. Spectrosc. 204 (2018) 568–575, https://doi.org/10.1016/j.saa.2018.06.068.
[39] D.H. Cai, C.L. Zhang, Q.Y. Liu, L. He, Y.J. Liu, Y.H. Xiong, X.Y. Le, Synthesis, DNA binding, antibacterial and anticancer properties of two novel water-soluble copper(II) complexes containing gluconate, Eur. J. Med. Chem. 213 (2021) 113182, https://doi.org/10.1016/j.ejmech.2021.113182.
[40] N. Ganji, A. Rambabu, N. Vamsikrishna, S. Daravath, Shivaraj, Copper(II) complexes with isoxazole Schiff bases: Synthesis, spectroscopic investigation, DNA binding and nuclease activities, antioxidant and antimicrobial studies, J. Mol. Struct. 1173 (2018) 173–182, https://doi.org/10.1016/j.molstruc.2018.06.100.
[41] W. Zhou, X. Wang, M. Hu, C. Zhu, Z. Guo, A mitochondrion-targeting copper complex exhibits potent cytotoxicity against cisplatin-resistant tumor cells through multiple mechanisms of action, Chem. Sci. 5 (2014) 2761–2770, https://doi.org/10.1039/c4sc00384e.
[42] S. Tabassum, M. Ahmad, M. Afzal, M. Zaki, P.K. Bharadwaj, Synthesis and structure elucidation of a copper(II) Schiff-base complex: In vitro DNA binding, pBR322 plasmid cleavage and HSA binding studies, J. Photochem. Photobiol. B Biol. 140 (2014) 321–331, https://doi.org/10.1016/j.jphotobiol.2014.08.015.
[43] X. Wu, H. Li, Y. Kan, B. Yin, A regeneratable and highly selective fluorescent probe for sulfide detection in aqueous solution, Dalton Trans. 42 (2013) 16302–16310, https://doi.org/10.1039/c3dt51953h.
[44] S. Palanisamy, L.Y. Lee, Y.L. Wang, Y.J. Chen, C.Y. Chen, Y.M. Wang, A water soluble and fast response fluorescent turn-on copper complex probe for H_2S detection in zebra fish, Talanta 147 (2016) 445–452, https://doi.org/10.1016/j.talanta.2015.10.019.
[45] M.-Q. Wang, K. Li, J.-T. Hou, M.-Y. Wu, Z. Huang, X.-Q. Yu, BINOL-Based Fluorescent Sensor for Recognition of Cu(II) and Sulfide Anion in Water, J. Org. Chem. 77 (2012) 8350–8354.
[46] P. Wang, J. Wu, C. Di, R. Zhou, H. Zhang, P. Su, C. Xu, P. Zhou, Y. Ge, D. Liu, W. Liu, Y. Tang, A novel peptide-based fluorescence chemosensor for selective imaging of hydrogen sulfide both in living cells and zebrafish, Biosens. Bioelectron. 92 (2017) 602–609, https://doi.org/10.1016/j.bios.2016.10.050.
[47] H.M. Chawla, P. Goel, P. Munjal, A new metallo-supramolecular sensor for recognition of sulfide ions, Tetrahedron Lett. 56 (2015) 682–685, https://doi.org/10.1016/j.tetlet.2014.12.057.
[48] C.H. Min, S. Na, J.E. Shin, J.K. Kim, T.G. Jo, C. Kim, A new Schiff-based chemosensor for chromogenic sensing of Cu^{2+}, Co^{2+} and S^{2-} in aqueous solution: experimental and theoretical studies, New J. Chem. 41 (2017) 3991–3999, https://doi.org/10.1039/c7nj00054e.
[49] Y.L. Pak, J. Li, K.C. Ko, G. Kim, J.Y. Lee, J. Yoon, Mitochondria-Targeted Reaction-Based Fluorescent Probe for Hydrogen Sulfide, Anal. Chem. 88 (2016) 5476–5481, https://doi.org/10.1021/acs.analchem.6b00956.
[50] D. Das, S. Sutradhar, K. Rissanen, B.N. Ghosh, Synthesis and Structure of Trimethylplatinum(IV) Iodide Complex of 4'-(4-Methoxyphenyl)-2,2':6',2''-terpyridine Ligand and its Halogen Bonding Property, Z. anorg. allg. Chem. 646 (2020) 301–306, https://doi.org/10.1002/zaac.201900201.
[51] B.N. Ghosh, M. Lahtinen, E. Kalenius, P. Mal, K. Rissanen, 2,2′:6′,2″-Terpyridine Trimethylplatinum(IV) Iodide Complexes as Bifunctional Halogen Bond Acceptors, Cryst. Growth Des. 16 (2016) 2527–2534, https://doi.org/10.1021/acs.cgd.5b01552.
[52] P. Sarkar, S. Gupta, A.H.U. Kumar, D. Das, S. Sutradhar, K. Paul, N.K. Lokanath, B.N. Ghosh, Protein interactions and drug displacement studies of novel copper (II) and zinc(II) complexes of a dipyrazinylpyridine ligand, J. Mol. Liq. 387 (2023) 122561, https://doi.org/10.1016/j.molliq.2023.122561.
[53] S. Sutradhar, D. Das, B.N. Ghosh, Copper(II) and Cadmium(II) triggered hydrogelation of a simple trimethoxy terpyridine ligand, J. Mol. Struct. 1265 (2022) 133442, https://doi.org/10.1016/j.molstruc.2022.133442.
[54] S. Sutradhar, S. Basak, D. Das, B.N. Ghosh, Hydrogelation behaviour of methoxy terpyridine ligand induced by transition metal ions, Polyhedron 236 (2023) 116344, https://doi.org/10.1016/j.poly.2023.116344.
[55] B.N. Ghosh, S. Bhowmik, P. Mal, K. Rissanen, A highly selective, Hg^{2+} triggered hydrogelation: Modulation of morphology by chemical stimuli, Chem. Commun. 50 (2014) 734–736, https://doi.org/10.1039/c3cc47591c.
[56] D. Das, R.M. Gomila, P. Sarkar, S. Sutradhar, A. Frontera, B.N. Ghosh, Novel Zn-dppy based receptor for selective sensing of pyrophosphate anion in aqueous acetonitrile medium, Polyhedron 223 (2022) 115959, https://doi.org/10.1016/j.poly.2022.115959.
[57] D. Das, S. Sutradhar, R.M. Gomila, K. Rissanen, A. Frontera, B.N. Ghosh, Synthesis, structure and application of a simple cadmium(II)-terpyridine complex as sensor material for selective detection of pyrophosphate anion, J. Mol. Struct. 1273 (2023) 134269, https://doi.org/10.1016/j.molstruc.2022.134269.
[58] K. Velugula, J.P. Chinta, Silver nanoparticles ensemble with Zn(II) complex of terpyridine as a highly sensitive colorimetric assay for the detection of Arginine, Biosens. Bioelectron. 87 (2017) 271–277, https://doi.org/10.1016/j.bios.2016.08.023.
[59] S. Bhowmik, B.N. Ghosh, V. Marjomäki, K. Rissanen, Nanomolar pyrophosphate detection in water and in a self-assembled hydrogel of a simple terpyridine-Zn^{2+} complex, J. Am. Chem. Soc. 136 (2014) 5543–5546, https://doi.org/10.1021/ja4128949.
[60] B.N. Ghosh, F. Topić, P.K. Sahoo, P. Mal, J. Linnera, E. Kalenius, H.M. Tuononen, K. Rissanen, Synthesis, structure and photophysical properties of a highly luminescent terpyridine-diphenylacetylene hybrid fluorophore and its metal complexes, Dalton Trans. 44 (2015) 254–267, https://doi.org/10.1039/c4dt02728k.
[61] D. Das, S. Sutradhar, A. Singh, B.N. Ghosh, Zinc-Terpyridine Based Chemosensor for Detection of Pyrophosphate Anion in Aqueous Medium, Z. anorg. allg. Chem. 647 (2021) 1234–1238, https://doi.org/10.1002/zaac.202100054.
[62] C. Giuriati, S. Cavalli, A. Gorni, D. Badocco, P. Pastore, Ion chromatographic determination of sulfide and cyanide in real matrices by using pulsed amperometric detection on a silver electrode, J. Chromatogr. A 1023 (2004) 105–112, https://doi.org/10.1016/j.chroma.2003.10.001.
[63] K. Han, W.F. Koch, Determination of Sulfide at the Parts-per-Billion Level by Ion Chromatography with Electrochemical Detection, Anal. Chem. 59 (1987) 1016–1020, https://doi.org/10.1021/ac00134a019.
[64] J. Rodríguez-Fernández, J. Manuel Costa, R. Pereiro, A. Sanz-Medel, Simple detector for oral malodour based on spectrofluorimetric measurements of hydrogen sulphide in mouth air, Anal. Chim. Acta 398 (1999) 23–31, https://doi.org/10.1016/S0003-2670(99)00381-5.
[65] B. Spilker, J. Randhahn, H. Grabow, H. Beikirch, P. Jeroschewski, New electrochemical sensor for the detection of hydrogen sulfide and other redox active species, J. Electroanal. Chem. 612 (2008) 121–130, https://doi.org/10.1016/j.jelechem.2007.09.019.
[66] J. Chen, Y. Zhang, S. Miao, M. Wang, B. Yang, An accurate and portable colorimetric chemosensor for S^{2-} detection *via* two complementary mechanisms, New J. Chem. 44 (2020) 12579–12585, https://doi.org/10.1039/d0nj02544e.
[67] B. Sinduja, S.A. John, Silver nanoparticles capped with carbon dots as a fluorescent probe for the highly sensitive "off–on" sensing of sulfide ions in water, Anal. Bioanal. Chem. 411 (2019) 2597–2605, https://doi.org/10.1007/s00216-019-01697-2.
[68] M. Vora, S. Dey, A. Kongor, M. Panchal, F. Panjwani, A. Verma, V. Jain, An oxacalix[4]arene-derived dual-sensing fluorescent probe for the relay recognition of Hg^{2+} and S^{2-} ions, New J. Chem. 45 (2021) 17902–17908, https://doi.org/10.1039/d1nj03953a.
[69] J. Palion-Gazda, B. Machura, T. Klemens, A. Szlapa-Kula, S. Krompiec, M. Siwy, H. Janeczek, E. Schab-Balcerzak, J. Grzelak, S. Maćkowski, Structure-dependent and environment-responsive optical properties of the trisheterocyclic systems

with electron donating amino groups, Dyes Pigments 166 (2019) 283–300, https://doi.org/10.1016/j.dyepig.2019.03.035.
[70] P. Sinha, N. Kumari, K. Singh, K. Singh, L. Mishra, Homoleptic bisterpyridyl complexes: Synthesis, characterization, DNA binding, DNA cleavage and topoisomerase II inhibition activity, Inorg. Chim. Acta 432 (2015) 71–80, https://doi.org/10.1016/j.ica.2015.03.026.
[71] S.G. Vincent, R.R.K. Jyothi, J. Joseph, Novel metal complexes of flavone Schiff base : Synthesis , characterization , antioxidant and DNA binding studies, Mater. Today Proc. 45 (2021) 1031–1038, https://doi.org/10.1016/j.matpr.2020.03.141.
[72] A. Wolfe, G.H. Shimer Jr., T. Meehan, Polycyclic aromatic hydrocarbons physically intercalate into duplex regions of denatured DNA, Biochem. 26 (1987) 6392–6396, https://doi.org/10.1021/bi00394a013.
[73] K. Choroba, B. Machura, A. Szlapa-Kula, J.G. Malecki, L. Raposo, C. Roma-Rodrigues, S. Cordeiro, P.V. Baptista, A.R. Fernandes, Square planar Au(III), Pt(II) and Cu(II) complexes with quinoline-substituted 2,2′:6′,2″-terpyridine ligands: From in vitro to in vivo biological properties, Eur. J. Med. Chem. 218 (2021) 113404, https://doi.org/10.1016/j.ejmech.2021.113404.
[74] W.W. Fu, D. Peng, Y.Q. Li, J.R. Shen, S.H. Li, Syntheses, crystal structures and DNA-binding activities of divalent Fe, Cu, Zn and Cd complexes with 4′-(furan-2-yl)-2,2′:6′,2″-terpyridine, Z. Naturforsch. 72 (2017) 687–695, https://doi.org/10.1515/znb-2017-0041.
[75] R. Masnikosa, M.M. Milutinović, I. Crnolatac, A. Tot, S. Veličković, Ž. Bojić-Trbojević, A. Rilak-Simović, Anti-adhesive action of novel ruthenium(II) chlorophenyl terpyridine complexes with a high affinity for double-stranded DNA: *in vitro* and *in silico*, J. Inorg. Biochem. 208 (2020) 111090, https://doi.org/10.1016/j.jinorgbio.2020.111090.
[76] S. Ghosh, Z. Abbas, S. Dasari, A.K. Patra, Luminescent Eu^{3+} and Tb^{3+} complexes of 4-aminophenyl terpyridine (ptpy): Photophysical aspects, DNA and serum protein binding properties, J. Lumin. 187 (2017) 46–52, https://doi.org/10.1016/j.jlumin.2017.02.063.
[77] C. Balakrishnan, S. Natarajan, M.A. Neelakantan, Exploration of biological activities of alkyne arms containing Cu(II) and Ni(II) complexes: Syntheses, crystal structures and DFT calculations, RSC Adv. 6 (2016) 102482–102497, https://doi.org/10.1039/c6ra20650f.
[78] J. Fan, A. Fu, L. Zhang, Progress in molecular docking, Quant. Biol. 7 (2019) 83–89, https://doi.org/10.1007/s40484-019-0172-y.
[79] Dassault Systèmes BIOVIA, Discovery Studio Visualizer, BIOVIA Discovery Studio Visualizer n.d.) V21.1.0.20298 (2021). http://accelrys.com.
[80] M.J. Frisch, G.W. Trucks, H.B. Schlegel, G.E. Scuseria, M.A. Robb, J.R. Cheeseman, G. Scalmani, V. Barone, B. Mennucci, G.A. Petersson, H. Nakatsuji, M. Caricato, X. Li, H.P. Hratchian, A.F. Izmaylov, J. Bloino, G. Zheng, J.L. Sonnenberg, M. Hada, M. Ehara, K. Toyota, R. Fukuda, J. Hasegawa, M. Ishida, T. Nakajima, Y. Honda, O. Kitao, H. Nakai, T. Vreven, J.A. Montgomery, J.E. Peralta, F. Ogliaro, M. Bearpark, J.J. Heyd, E. Brothers, K.N. Kudin, V.N. Staroverov, R. Kobayashi, J. Normand, K. Raghavachari, A. Rendell, J.C. Burant, S.S. Iyengar, J. Tomasi, M. Cossi, N. Rega, J.M. Millam, M. Klene, J.E. Knox, J.B. Cross, V. Bakken, C. Adamo, J. Jaramillo, R. Gomperts, R.E. Stratmann, O. Yazyev, A.J. Austin, R. Cammi, C. Pomelli, J.W. Ochterski, R.L. Martin, K. Morokuma, V.G. Zakrzewski, G.A. Voth, P. Salvador, J.J. Dannenberg, S. Dapprich, A.D. Daniels, Farkas, J.B. Foresman, J. V Ortiz, J. Cioslowski, D.J. Fox, Gaussian 16, Revision C.01, Gaussian, Inc., Wallingford CT, 2016.
[81] D. Das, A. Roy, S. Sutradhar, F. Fantuzzi, B.N. Ghosh, A simple copper(II) dppy-based receptor for sensing of l-cysteine and l-histidine in aqueous acetonitrile medium, Sens. Diagn. 2 (2023) 1649–1657, https://doi.org/10.1039/d3sd00183k.
[82] C. Adamo, V. Barone, Toward reliable density functional methods without adjustable parameters: The PBE0 model, J. Chem. Phys. 110 (1999) 6158–6170, https://doi.org/10.1063/1.478522.
[83] M. Ernzerhof, G.E. Scuseria, Assessment of the Perdew–Burke–Ernzerhof exchange-correlation functional, J. Chem. Phys. 110 (1999) 5029–5036, https://doi.org/10.1063/1.478401.
[84] S. Grimme, J. Antony, S. Ehrlich, H. Krieg, A consistent and accurate ab initio parametrization of density functional dispersion correction (DFT-D) for the 94 elements H-Pu, J. Chem. Phys. 132 (2010) 154104, https://doi.org/10.1063/1.3382344.
[85] S. Grimme, S. Ehrlich, L. Goerigk, Effect of the damping function in dispersion corrected density functional theory, J. Comput. Chem. 32 (2011) 1456–1465, https://doi.org/10.1002/jcc.21759.
[86] F. Weigend, R. Ahlrichs, Balanced basis sets of split valence, triple zeta valence and quadruple zeta valence quality for H to Rn: Design and assessment of accuracy, Phys. Chem. Chem. Phys. 7 (2005) 3297–3305, https://doi.org/10.1039/b508541a.
[87] A.V. Marenich, C.J. Cramer, D.G. Truhlar, Universal Solvation Model Based on Solute Electron Density and on a Continuum Model of the Solvent Defined by the Bulk Dielectric Constant and Atomic Surface Tensions, J. Phys. Chem. B 113 (2009) 6378–6396, https://doi.org/10.1021/jp810292n.
[88] M. Sparta, C. Riplinger, F. Neese, Mechanism of Olefin Asymmetric Hydrogenation Catalyzed by Iridium Phosphino-Oxazoline: A Pair Natural Orbital Coupled Cluster Study, J. Chem. Theory Comput. 10 (2014) 1099–1108, https://doi.org/10.1021/ct400917j.
[89] R.L. Martin, P.J. Hay, L.R. Pratt, Hydrolysis of Ferric Ion in Water and Conformational Equilibrium, J. Phys. Chem. A 102 (1998) 3565–3573, https://doi.org/10.1021/jp980229p.
[90] F. Fantuzzi, M.A.C. Nascimento, B. Ginovska, R.M. Bullock, S. Raugei, Splitting of multiple hydrogen molecules by bioinspired diniobium metal complexes: A DFT study, Dalton Trans. 50 (2021) 840–849, https://doi.org/10.1039/d0dt03411h.
[91] T. Lu, F. Chen, Multiwfn: A multifunctional wavefunction analyzer, J. Comput. Chem. 33 (2012) 580–592, https://doi.org/10.1002/jcc.22885.
[92] F. Plasser, TheoDORE : A toolbox for a detailed and automated analysis of electronic excited state computations, J. Chem. Phys. 152 (2020) 084108, https://doi.org/10.1063/1.5143076.
[93] A.W. Addison, T.N. Rao, Synthesis, Structure, and Spectroscopic Properties of Copper(II) Compounds containing Nitrogen-Sulphur Donor Ligands ; the Crystal and Molecular Structure of Aqua[l,7-bis(N-methylbenzimidazol-2'-yl)- 2,6-dithiaheptane]copper(II) Perchlorate, J. Chem. Soc. Dalton Trans. (1984) 1349–1356, https://doi.org/10.1039/DT9840001349.
[94] K. Choroba, B. Machura, S. Kula, L.R. Raposo, A.R. Fernandes, R. Kruszynski, K. Erfurt, L.S. Shul'Pina, Y.N. Kozlov, G.B. Shul'Pin, Copper(II) complexes with 2,2′:6′,2″-terpyridine, 2,6-di(thiazol-2-yl)pyridine and 2,6-di(pyrazin-2-yl)pyridine substituted with quinolines. Synthesis, structure, antiproliferative activity, and catalytic activity in the oxidation of alkanes and alcohols, Dalton Trans. 48 (2019) 12656–12673, https://doi.org/10.1039/c9dt01922g.
[95] H.R. Khavasi, M. Esmaeili, Is Gelation Behavior Predictable through a Crystal Engineering Approach? A Case Study in Four Similar Coordination Compounds, Langmuir 35 (2019) 4660–4671, https://doi.org/10.1021/acs.langmuir.9b00027.
[96] L. Li, Y.Z. Zhang, C. Yang, E. Liu, J.C. Fettinger, G. Zhang, Two polymorphs of 4-(4-hexyloxyphenyl)-2,6-di(pyrazin-2-yl)pyridine and the crystal structure of its copper(II) complex, J. Mol. Struct. 1110 (2016) 19–23, https://doi.org/10.1016/j.molstruc.2016.01.024.
[97] U. Diwan, V. Kumar, R.K. Mishra, N.K. Rana, B. Koch, K.K. Upadhyay, Harvesting red fluorescence through design specific tuning of ICT and ESIPT: An efficient optical detection of cysteine and live cell imaging, RSC Adv. 6 (2016) 95722–95728, https://doi.org/10.1039/c6ra18093k.
[98] D. Das, P. Sarkar, A.H.U. Kumar, S. Sutradhar, M. Kotakonda, N.K. Lokanath, B. N. Ghosh, Nanomolar pyrophosphate detection in water using a zinc-terpyridine receptor and its applications in antiproliferative and antioxidant activity, J. Photochem. Photobiol. A Chem. 441 (2023) 114726, https://doi.org/10.1016/j.jphotochem.2023.114726.
[99] P. Wei, L. Xiao, Y. Gou, F. He, P. Wang, X. Yang, A novel peptide-based relay fluorescent probe with a large Stokes shift for detection of Hg^{2+} and S^{2-} in 100 % aqueous medium and living cells: Visual detection via test strips and smartphone, Spectrochim. Acta A Mol. Biomol. Spectrosc. 285 (2023) 121836, https://doi.org/10.1016/j.saa.2022.121836.
[100] S. Tantubay, H. Kalita, A. Pathak, Sensitive detection of auric and sulphide ions using hybrid silver/nitrogen-doped carbon nanoparticles, Sens. Actuators B Chem. 330 (2021) 129276, https://doi.org/10.1016/j.snb.2020.129276.
[101] J. Chen, Y. Li, K. Lv, W. Zhong, H. Wang, Z. Wu, P. Yi, J. Jiang, Cyclam-functionalized carbon dots sensor for sensitive and selective detection of copper (II) ion and sulfide anion in aqueous media and its imaging in live cells, Sens. Actuators B Chem. 224 (2016) 298–306, https://doi.org/10.1016/j.snb.2015.10.046.
[102] J. Yang, Y. Zhang, L. Li, H. Cao, W. Qu, L. Jia, A quinolimide-based reversible fluorescent sensor for Cu^{2+} and S^{2-} and its applications, J. Mol. Struct. 1275 (2023) 134638, https://doi.org/10.1016/j.molstruc.2022.134638.
[103] L. Xiao, P. Wei, F. He, Y. Gou, Y. Ge, Y. Liu, P. Wang, Peptide-based fluorescent and colorimetric dual-functional probe for visual detection of Cu^{2+} , Hg^{2+} and S^{2-} in 100% aqueous media, living cells and paper test strips, J. Photochem. Photobiol. A Chem. 433 (2022) 114178, https://doi.org/10.1016/j.jphotochem.2022.114178.
[104] B. Anupama, DNA binding interactions, docking and antioxidative studies of ternary copper (II) complexes, J. Mol. Struct. 1210 (2020) 127988, https://doi.org/10.1016/j.molstruc.2020.127988.
[105] V.T. Yilmaz, C. Icsel, F. Suyunova, M. Aygun, B. Cevatemre, E. Ulukaya, Synthesis, structures, DNA/protein binding, molecular docking, anticancer activity and ROS generation of Ni(II), Cu(II) and Zn(II) 5,5-diethylbarbiturate complexes with bis(2-pyridylmethyl)amine and terpyridine, New J. Chem. 41 (2017) 8092–8106, https://doi.org/10.1039/c7nj00887b.
[106] B. Kaya, Z.K. Yılmaz, O. Şahin, B. Aslim, Ü. Tükenmez, B. Ülküseven, Structural analysis and biological functionalities of iron(III)– and manganese(III)–thiosemicarbazone complexes: in vitro anti-proliferative activity on human cancer cells, DNA binding and cleavage studies, J. Biol. Inorg. Chem. 24 (2019) 365–376, https://doi.org/10.1007/s00775-019-01653-6.
[107] S. Dasari, S. Singh, Z. Abbas, S. Sivakumar, A.K. Patra, Luminescent lanthanide (III) complexes of DTPA-bis(amido-phenyl-terpyridine) for bioimaging and phototherapeutic applications, Spectrochim. Acta A Mol. Biomol. Spectrosc. 256 (2021) 119709, https://doi.org/10.1016/j.saa.2021.119709.
[108] Y.-X. Liu, H.-W. Mo, Z.-Y. Lv, F. Shen, C.-L. Zhang, Y.-Y. Qi, Z.-W. Mao, X.-Y. Le, DNA binding , crystal structure , molecular docking studies and anticancer activity evaluation of a copper (II) complex, Transit. Met. Chem. 43 (2018) 259–271, https://doi.org/10.1007/s11243-018-0211-y.

[109] J. Liu, T. Zhang, T. Lu, L. Qu, H. Zhou, Q. Zhang, L. Ji, D NA-binding and cleavage studies of macrocyclic copper (II) complexes, J. Inorg. Biochem. 91 (2002) 269–276, https://doi.org/10.1016/S0162-0134(02)00441-5.
[110] V.M. Manikandamathavan, M. Thangaraj, T. Weyhermuller, R.P. Parameswari, V. Punitha, N.N. Murthy, B.U. Nair, Novel mononuclear Cu (II) terpyridine complexes: Impact of fused ring thiophene and thiazole head groups towards DNA/BSA interaction, cleavage and antiproliferative activity on HepG2 and triple negative CAL-51 cell line, Eur. J. Med. Chem. 135 (2017) 434–446, https://doi.org/10.1016/j.ejmech.2017.04.030.
[111] M. Medjedović, A.R. Simović, D. Ćoćić, M. Milutinović, L. Senft, S. Blagojević, N. Milivojević, B. Petrović, Dinuclear ruthenium(II) polypyridyl complexes: Mechanistic study with biomolecules, DNA/BSA Interactions and Cytotoxic Activity, Polyhedron 178 (2020) 114334, https://doi.org/10.1016/j.poly.2019.114334.